Spacecraft Rendezvous with Non-Linear Dual-Quaternion Controller Under Orbital Perturbations

Thomas Key

A thesis
submitted in partial fulfillment of the
requirements for the degree of

Master of Science in Aeronautics & Astronautics

University of Washington

2025

Committee:
Mehran Mesbahi
Carl Knowlen

Program Authorized to Offer Degree:
William E. Boeing Department of Aeronautics and Astronautics

University of Washington

Abstract

Spacecraft Rendezvous with Non-Linear Dual-Quaternion Controller Under Orbital Perturbations

Thomas Key

Chair of the Supervisory Committee:
Mehran Mesbahi
William E. Boeing Department of Aeronautics and Astronautics

A non-linear control system based on several controllers is applied the satellite rendezvous problem with a dual quaternion framework. The spacecraft pose is simulated under the effects of typical orbital perturbations with some initial proximity already established in advance. The objective is to present an approach to the rendezvous and proximity operations problem with the addition of attitude constraints using control barrier functions and dual quaternion feedback. Such applications with dual quaternions may also be applied to planetary descent and landing, six degree of freedom simulation, video graphics, and robotic pose control.

TABLE OF CONTENTS

Page

List of Figures iii

Glossary v

Chapter 1: Introduction and Motivation 1
1.1 A Brief Treatise on Quaternions and Applications in Space 4
1.2 Structure of Thesis 6

Chapter 2: Preliminary in Ordinary and Dual Quaternions 8
2.1 Clifford Algebra Formulation 8
2.2 Rotations and Operations with Quaternions 10
2.3 Translation and Dual Quaternion Operations 13
2.4 Frames of Reference with Dual Quaternions 16

Chapter 3: System Dynamics and Model Development 19
3.1 Dual Quaternion Dynamics 19
3.2 Orbital Perturbations and Test Conditions 26

Chapter 4: Control Law Formulation 33
4.1 Dual Quaternion Feedback Control Methodology 33
4.2 Dual PD Controller Formulation 33
4.3 Non-Linear Control via Back-stepping and Lyapunov Stability 35
4.4 Synthesis of Controller 40

Chapter 5: Results and Analysis 42
5.1 LEO Case 43
5.2 Maratus Case 47
5.3 Limitations of Methodology and Future Work 52

Bibliography 53

Appendix A: Derivation/Proof of $\boldsymbol{M}(\boldsymbol{\theta_C})$ 57

Appendix B: Positive Definiteness for Hessian of Control Barrier Function 59

Appendix C: Additional Graphical Results 62

LIST OF FIGURES

Figure Number		Page
1.1	Line-Of-Sight Rendezvous [1]	2
1.2	"Commuter" Spacecraft in Early Rendezvous Method Developments [6]	3
1.3	Varying launch direction from spacecraft with $10\frac{\text{ft}}{\text{s}}$ initial speed [11]	4
1.4	Visual representation of thesis flow with sources	6
2.1	Matrix representation of rotation in $\mathbb{R}^3$	10
2.2	Axis-angle representation of rotation	12
2.3	Reference frames as relative poses	14
2.4	Geocentric equatorial frame definition	16
2.5	Body frame definition, with comms. ($\mathcal{C}$) frame and reaction wheel ($\mathcal{R}$) frames.	17
3.1	Dual Momentum $\mathcal{H}$ as a combination of linear and angular velocities.	23
3.2	Dual Wrench $\tilde{\boldsymbol{f}}$ as a combination of forces and moments on a body.	24
3.3	J_2 effects on a satellite in orbit.	27
3.4	Surface area considerations for $\mathcal{A}$ frame and drag calculations.	29
3.5	LEO orbit case	32
3.6	Maratus orbit case	32
5.1	LEO case with PD: Velocities over time	43
5.2	LEO case with CBF: Velocities over time	44
5.3	LEO case with combined controller: Velocities over time	45
5.4	Comparison of control efforts in selected axes	46
5.5	k_p vs. $\|\vec{r}^{\mathcal{B}}_{B/G}\|$: PD Controller	47
5.6	$\|\vec{r}^{\mathcal{B}}_{B/G}\|$ vs. k_p and k_d for combined controller	48
5.7	$\|\vec{\tau}^{\mathcal{B}}_{c}\|$ vs. k_{CBF} for combined controller and CBF	49
5.8	Maratus Case with combined controller: Velocities over time	50
5.9	$\boldsymbol{q}_{B/G}$ for Combined Controller and CBF	51
C.1	Control comparison in $\mathcal{B}_x$ and $\mathcal{B}_y$: LEO	62

C.2 Control torque comparison in $\mathcal{B}_z$ and $\mathcal{B}_y$: LEO 63
C.3 Maratus Case with PD controller: Velocities over time 63
C.4 Maratus Case with CBF: Velocities over time 64

GLOSSARY

ATTITUDE: The orientation in space of a vehicle or reference frame with respect to some inertial frame.

BORESIGHT: A unit direction vector emanating from some sensitive component such as a camera or antenna.

DUAL QUATERNION: A composition of two ordinary quaternions, with one scaled by the dual number ε.

GIMBAL LOCK: A phenomena wherein two axes align with one another in an attitude determination scheme, preventing it from being determined at all.

LYAPUNOV FUNCTION: A scalar valued function $V(x)$ satisfying $V(x) > 0$ and $\dot{V}(x) < 0$ for all $x \neq 0$ where $V(0) = 0$. Used to show stability in non-linear systems.

ORDINARY QUATERNION: The family of unit quaternions with non-zero scalar part.

PURE QUATERNION: The set of ordinary quaternions with zero scalar part, analogous to a vector in $\mathbb{R}^3$.

RENDEZVOUS: The process of connecting or otherwise making contact with another vehicle in space. C'est aussi écrit comme «rendez-vous».

SLEW: A synonym for the attitude or orientation of a satellite.

STATION-KEEP: The process of maintaining a relative position with another satellite or maintaining a keplerian orbit.

QUATERNION: A value in $\mathbb{H}$ represented as a 4×1 vector used to rotate vectors in $\mathbb{R}^3$.

6DOF: An acronym for six degree-of-freedom.

ACKNOWLEDGMENTS

The unyielding support of my parents Janette Key and Charles Key III is what gave me the tools I needed to pursue my education. I love you both dearly. To my colleagues and friends John Nguyen, Kyle Fisher, Caroline Baxter, Taylour Mills, Seven Bennett, Shuba Murthy, Nithin Adidela, Guadalupe Guadarrama, Ainaz Eftekhar, Eomji Kim, Shavy Kashyap and Mason Green, thank you for your support in every possible sense. Of course, I would also like to thank my advisor Mehran Mesbahi, for being very patient with me in my academic pursuits in writing this work.

I made so many lovely memories inside the Kirsten Wind Tunnel, thank you to everybody there for bearing with me and keeping me sharp. To the wonderful cohort I had the pleasure of teaching during my final academic year, thank you for your kind and motivating words. Professors Eduardo Viana da Silva and Fábio de Oliveira Fialho, thank you for your continued faith in me and your support in broadening my horizons internationally. Muitíssimo obrigado, vocês mudaram minha vida. Finally, I would like to thank Café Allegro, Bulldog News, and Café on the Ave for their unyielding aid. *Per aspera ad astra.*

DEDICATION

To Eleanor, Esther, and Mary. Being your brother is a joy, as it always has been.

NOMENCLATURE

$\mathcal{A}, \mathcal{B}, \cdots, \mathcal{Z}$	Reference Frames
$\vec{a}$	Vector in $\mathbb{R}^3$
$\dot{\vec{a}}$	Derivative w.r.t time
$\mathbf{q}$	Quaternion ($\mathbb{H}$)
q_s	Scalar component of quaternion
$\vec{q}_v$	Vector component of quaternion
ε	Dual number ($\varepsilon^2 = 0$)
$\tilde{\mathbf{q}}$	Dual quaternion
$\tilde{\mathbf{q}}^*$	General quaternion conjugate
$\vec{a}^{\mathcal{B}}$	$\mathbb{R}^3$ Vector in $\mathcal{B}$ frame
$\vec{r}^{\mathcal{T}}_{B/I}$	Position of $\mathcal{B}$ w.r.t $\mathcal{I}$, in $\mathcal{T}$ frame
$\mathbf{q}_{B/I}$	Orientation of $\mathcal{B}$ w.r.t $\mathcal{I}$
$\tilde{\mathbf{q}}_{B/I}$	Pose of $\mathcal{B}$ w.r.t $\mathcal{I}$
$M_{B/I}$	Matrix representation of $\mathbf{q}_{B/I}$
$[M]$	$\mathbb{R}^{3\times3}$ matrix expressed in $\mathbb{R}^{4\times4}$
$\tilde{\boldsymbol{\omega}}$	Dual velocity or Motor
$\mathcal{H}$	Dual momentum
$\boldsymbol{f}$	Dual force or Wrench
$\mathbb{R}$	Set of real numbers
$\mathbb{H}$	Hamiltonian algebra, quaternions

Chapter 1

INTRODUCTION AND MOTIVATION

Rendezvous and proximity operations in an aerospace setting can be traced back to the beginning of heavier-than-air aviation, by pilots guiding small aircraft and even hot air balloons in unison or in proximity to one another in the sky. The first instances were performed at airshows in the 1920's, becoming commonplace in only a few short years. From there, the control of flight vehicles was relegated to straight and level flights with the aid of gyroscopes and hydraulic equipment. These innovations initially developed on Earth naturally transitioned to the space environment.

The first rendezvous of space vehicles is widely considered to be Gemini VI and Gemini VII in 1965, achieved without active control. The completion of which led the way to the maneuvers that championed the Apollo program. The first *autonomous* rendezvous and docking of two spacecraft occurred between Cosmos 186 and 188 in 1967, marking the first instance of its kind in space. This began the development of rendezvous as an astrospace engineering problem with the first instances completed in the 1960's generally as manual maneuvers performed by pilots [1, 6, 11]. Figure 1.1 shows the process for manual line-of-sight rendezvous, the standard at the time.

Methods for autonomously achieving rendezvous without the need for human input was being developed at the time but took time to be fully adopted at NASA. The general idea for autonomous rendezvous and docking is, of course, to align some position and/or orientation with another desired location in space. Frequently, the attitude and position of the spacecraft are treated as separate systems despite the coupling of the translational movement with the rotational state in the frame being controlled. However in certain applications one system may not need a control system at all. As an example of this, the SiriusSats operated with

no attitude or position control on-board and were the first satellites launched *by hand* from the ISS in 2018. In some cases, the control of a satellite's position is often omitted for small vehicles like CubeSats due to the associated complexity and cost.

Solving the rendezvous problem has always been a multifaceted process. Many systems outside of the guidance, navigation, and control perspective must work together for rendezvous. In this vein, there is a breadth of material on the docking problem from a purely mechanical perspective, attempting to safely correct misalignments and - in crewed missions - ensure a pressurized seal to ensure crew safety. However in uncooperative cases where communication does not or cannot happen between the two satellites, certain considerations must be made with respect to the other body. These situations could include orbiting asteroids, other un-cooperative satellites, or space debris. These situations require algorithms to estimation the relative pose in space with cameras or other visual sensors when the target is an uncooperative agent. Discussion on this subject is presented in Chapter 4.

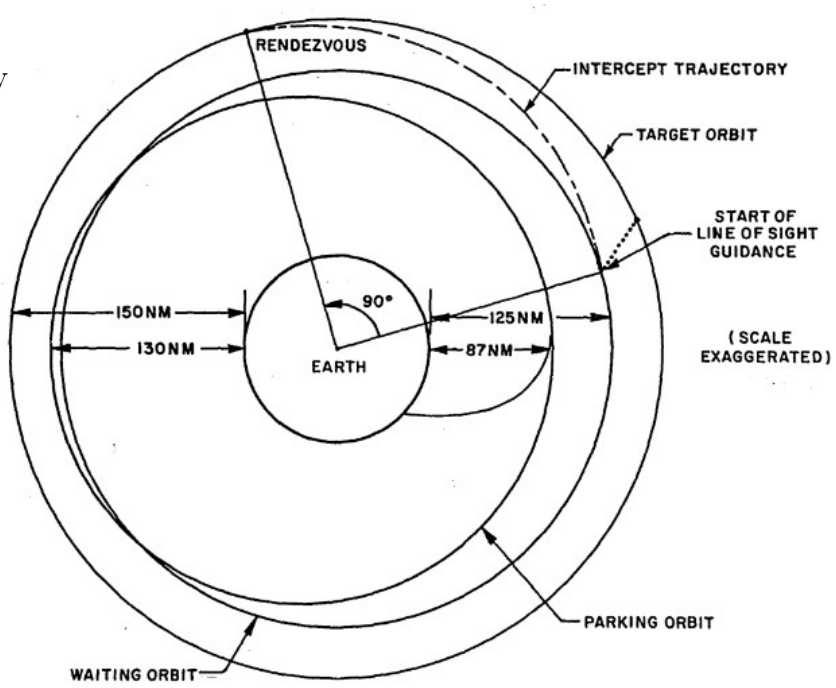

Figure 1.1: Line-Of-Sight Rendezvous [1]

The aforementioned rendezvous ($< 15\text{cm} - 30\text{cm}$) was during the Gemini program, and was performed *in advance* of the relative orbital dynamics being fully understood. The problem at that time was a practical one, where the proximity alone defined the metric for a

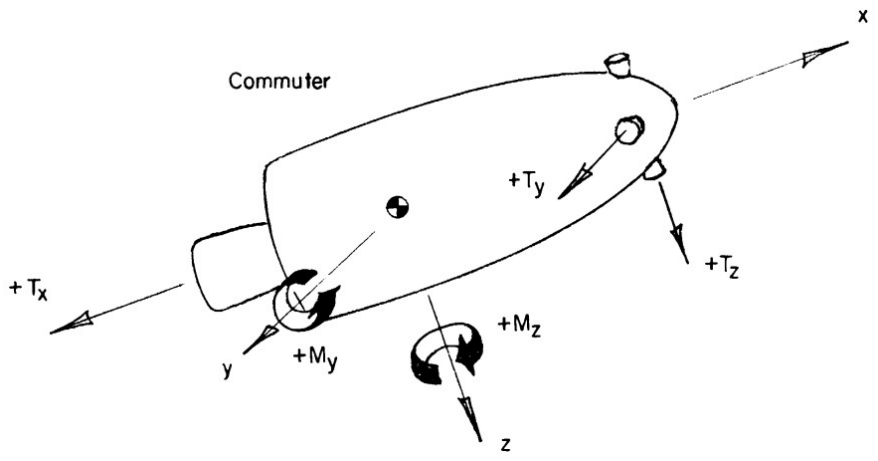

Figure 1.2: "Commuter" Spacecraft in Early Rendezvous Method Developments [6]

successful rendezvous. With the current number of satellites in orbit, the success of proximity operations may be measured differently. Oftentimes these metrics come from an optimality and safety perspective. This is to say, minimize fuel usage, avoid certain orientations and positions, or perform rendezvous in the least amount time. For the applications here, the majority of the discussion revolves around reducing control efforts for torque and thrust in Chapters 3 and 4 with some supporting material in Appendix B.

Proximity operations also suffer from a lack of natural intuition when moving relative to another mass in space. Figure 1.3 shows a set of paths traced out by masses launched from it with respect to the local reference frame. These paths do initially appear straight but over time appear to 'spiral' away from the original direction in which it was launched. In fact, this dynamic behavior is the same phenomena that caused first attempts at rendezvous to either fail or never fully achieve proximity. An example of this dissonance may be seen in the 'commuter' model presented in [6], shown in Figure 1.2 which included additional thrusters to aid in attitude control and provide tighter translational motion - a good design choice for rendezvous - yet did not take the orbital dynamics fully into consideration when published. Despite this, this general configuration was adopted for Gemini in its same year of publication.

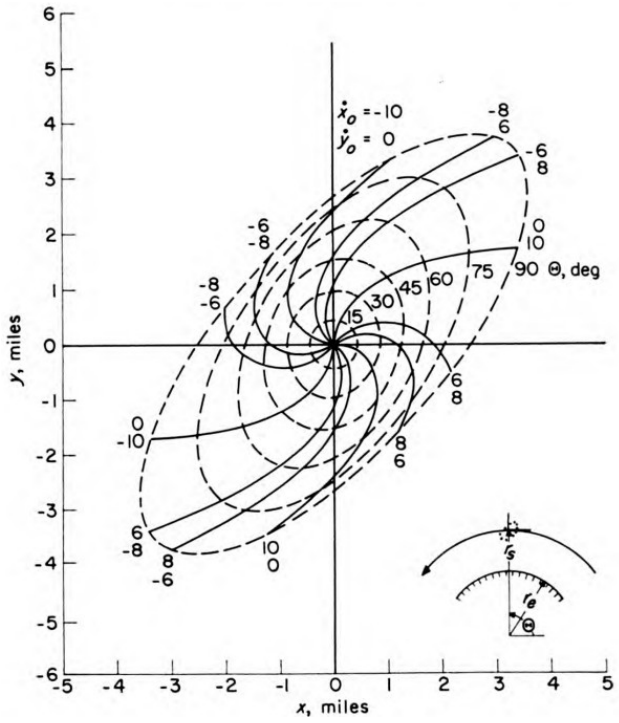

Figure 1.3: Varying launch direction from spacecraft with $10\frac{\text{ft}}{\text{s}}$ initial speed [11]

Now with methods such as model predictive control and convex optimization, proximity operations are becoming increasingly commonplace for problems such as formation flight or high speed re-orientation. The problem of rendezvous remains an active area of research, especially as the total number of satellites continues to increase. Since the signing of the Outer Space Treaties in 1967 the number of registered satellites in Low Earth Orbit (LEO) has skyrocketed. Approximately ten thousand satellites are currently in LEO as of 2025 [27, 20]. Growth in the space industry has also introduced satellite constellations on the order of a few dozen to a few thousand agents such as Iridium, Galileo, Starlink, and Kuiper. There is now an undeniable need for these satellites to interact with one another. A small satellite in LEO is the test case in Chapter 3, representative of the average modern satellite.

1.1 A Brief Treatise on Quaternions and Applications in Space

Michael Collins, the third and oft-omitted Astronaut of the Apollo 11 mission, joked that he wanted "a fourth gimbal for Christmas" while returning to Earth in July of 1969. This was due to *gimbal lock* within the on-board IMU. While a fourth gimbal could have partially alleviated the issue, a quaternion based IMU would have prevented the issue entirely. Quaternions would not be implemented at NASA until the Shuttle Program in 1981 [26, 7].

Dual quaternions have faced a slow rise to fame, but are currently receiving increasing attention from various industries such as robotics [16, 37], oncology [15], video graphics [19, 36, 37], and CNC machining [12]. Dual quaternions as applied in space have touched subjects such as pose estimation via the Dual-Quaternion Multiplicative-Extended-Kalman Filter (DQ-MEKF) [13, 14], planetary entry, descent, and landing [29], in-space robotics [31, 33], other kinematic models [16, 31], and motion constraints in rendezvous [10]. Ordinary quaternion based attitude control problems in general remain an active area of research as too, with nonlinear discrete-time [35], back-stepping [21, 23], lie-group based [18], and adaptive controllers [2] as recent examples. Versions of the attitude constraints have also been extended to dual quaternions in [24].

The application of dual quaternions can also be considered in the coupling the dynamics in a six degree-of-freedom model. From a classical standpoint, the rotational and translational components are considered separately with the result of one acting as an input to another. For example, cold gas thrusters set at a distance from its center of mass will provoke a torque in the system. Whether the rotation or translation as a result of the firing is calculated first may introduce small errors or delays in the system. These applications are well suited for dual quaternions as the combination of the dynamics permit a simultaneous consideration of the linear and angular components of the overall dynamics as a single combined system.

Quaternions, dual or otherwise, are an often under-appreciated method for transformations despite frequent use in practice. After being famously etched onto the side of a bridge in Ireland [8, 26, 29] the quaternions underwent a century of criticism. Despite this, both the the cross product and the word 'vector' originate from Hamilton's work on quaternions [8, 25]. At the time of their invention, other methods were more accessible until geometric algebra and modern computing shifted interest towards quaternions. This interest was motivated because quaternions offered a computationally cheap way to represent singularity-free rotation in $\mathbb{R}^3$. While quaternions weren't fully appreciated at first, the use of quaternions has now undeniably become an industry standard, a fourth gimbal for Christmas.

1.2 Structure of Thesis

The first chapter served as an introduction to spacecraft rendezvous as a modern application in industry, with some historical information relating to the the advent of the quaternion for attitude control. The technical discussion of the dual quaternion is left to Chapter 2, building on the ordinary quaternions. The rest of the thesis is expressed in totality here to guide the the development of the nonlinear dual quaternion controller. The general layout of the work is shown in Figure 1.4 as a visual aid with relevant sources for the following sections included. The second chapter will cover the relevant mathematical basis needed to develop the control law in Chapter 4. The preliminaries start with an emphasis on ordinary quaternions before introducing the dual quaternions. Important reference frames, the error quaternion, and other methods of rotation are presented as well.

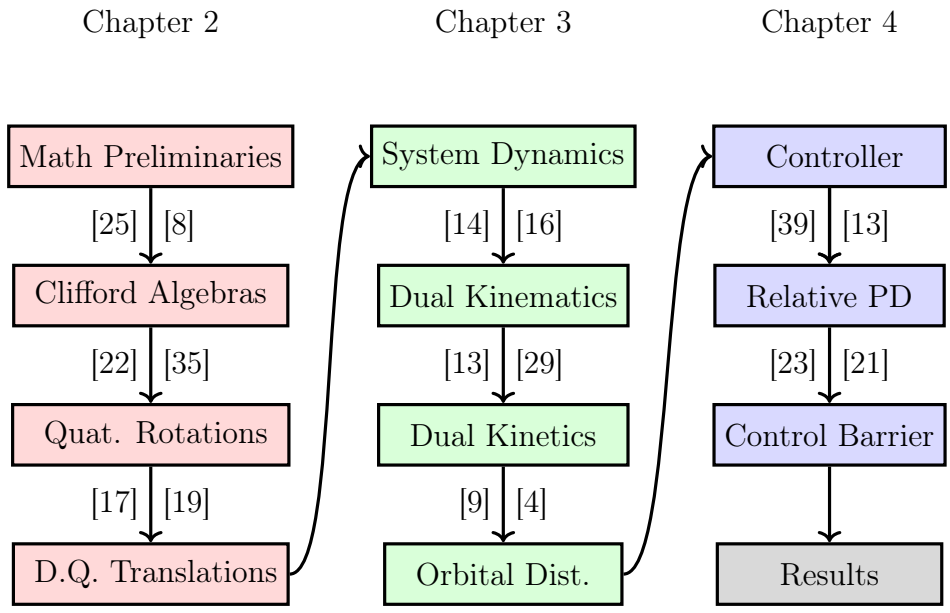

Figure 1.4: Visual representation of thesis flow with sources

Chapter 3 discusses and partially derives relevant dynamics for the simulated system with dual quaternions. The orbital perturbations are described with an emphasis on the method in which the drag forces are calculated as the formulation of drag is considered part of the contribution of this work, using dual quaternions to permit an aerodynamic center to be placed arbitrarily in the body for the calculation of the aerodynamic wrench. Chapter 4 covers the process for deriving the controller in two parts, the dual quaternion feedback PD controller, followed by the control barrier functions to include attitude constraints. In Chapter 5 numerical results are shown in comparison to the two controllers used to formulate the final controller. The simulation is performed under two orbital cases with a baseline set of conditions. Other graphical results are left in Appendix C.

Chapter 2

PRELIMINARY IN ORDINARY AND DUAL QUATERNIONS

The foundation for the quaternions is mathematically rich and is briefly presented here for completeness. On the historical front, the quaternions were developed by William Hamilton in the mid 17th century, extending the complex plane to what is now the Hamiltonian Algebra $\mathbb{H}$. The relevant structure of the quaternions and the dual quaternions are expressed here as a Clifford algebra. This formulation of quaternions and dual quaternions is presented analogous to [31].

2.1 Clifford Algebra Formulation

A Clifford algebra is an associative algebra defined over a vector space with a quadratic form as $x^2 = Q(x)\ \forall x \in \mathcal{X}$ with $\mathcal{X}$ as the vector space and Q as the quadratic form mapping $\mathcal{X}$ to a field. Expressing a Clifford algebra is usually done by $\mathrm{Cl}(s_1, s_2, s_3)(\mathcal{X}, Q)$ or in this application $\mathrm{Cl}(s_1, s_2, s_3)(\mathcal{X})$ with the values $\sum_i^3 s_i = \dim(\mathcal{X})$. For this work $\dim(\mathcal{X}) \neq \infty$, and the relevant vector space is $\mathbb{R}$, using $\mathrm{Cl}(s_2, s_3)(\mathbb{R})$ for this case.

The cases $\mathbb{R}^3$ and $\mathbb{R}^4$ the Clifford algebras are $\mathrm{Cl}(3,0)(\mathbb{R})$ and $\mathrm{Cl}(3,1)(\mathbb{R})$ respectively. Each will have their respective basis vectors $\{e_1, e_2, e_3\}$ and $\{e_1, e_2, e_3, e_4\}$ with $e_0 = 1$ for both as it is for all Clifford algebras. The basis elements for the spaces must satisfy

$$e_i^2 = \begin{cases} 1 & \forall i \in \{1, \cdots, s_1\} \\ -1 & \forall i \in \{s_1 + 1, \cdots, s_1 + s_2\} \\ 0 & \forall i \in \{s_1 + s_2 + 1, \cdots, \dim(\mathcal{X})\} \end{cases}$$

where the basis vectors are anti-commutative and span the Clifford algebra. These basis vectors for $\mathrm{Cl}(3,0)(\mathbb{R})$ will be the power set made of the vectors e_i. The basis vectors

are then $\{1, e_1, e_2, e_3, e_1e_2, e_1e_3, e_2e_3, e_1e_2e_3\}$. A linear combination of these values yields $q = q_0e_0 + q_\circ e_1 + q_\circ e_2 + q_\circ e_3 + q_1e_1e_2 + q_2e_1e_3 + q_3e_2e_3 + q_\circ e_1e_2e_3$. For closure the algebra must be even, therefore

$$q = q_0 + q_1e_1e_2 + q_2e_1e_3 + q_3e_2e_3$$
$$(e_1e_2)^2 = (e_1e_2)(e_1e_2) = -e_2e_1^2e_2 = -1 = i$$
$$\boldsymbol{q} = q_0 + q_1i + q_2j + q_3k$$

For dual quaternions the power set of basis vectors is $\{1, e_1, \cdots, e_1e_2e_3e_4\}$, with $e_1^2 = e_2^2 = e_3^2 = -1$ and $e_4^2 = 0$. By the same process the even subalgebra will have eight elements, the first of which are identical to the quaternion, and the rest a scaled quaternion. The intent of $\mathrm{Cl}(3,1)(\mathbb{R})$ is that the scaling factor is as follows

$$(e_1e_2e_3e_4)^2 = 0$$
$$e_1e_2e_3e_4 = \varepsilon$$

The value ε is the *dual number*. The dual number is frequently introduced conceptually by nilpotent matrices to make the concept more approachable, but taking the definition by axiom appears to be the preferable approach, somewhat analogous to the complex values [28]. The expression of a dual quaternion is then

$$\boxed{\tilde{\mathbf{q}} = \boldsymbol{q}_p + \varepsilon\boldsymbol{q}_d} \tag{2.1}$$

Where $\boldsymbol{q}_p$ and $\boldsymbol{q}_d$ are the ordinary part and the dual part of the dual quaternion.

2.2 Rotations and Operations with Quaternions

Rotations are most *intuitively* presented in $\mathbb{R}^3$ by a sequence of rotations performed as a composition of matrices. Each matrix defines a rotation by a given axis, and jointly perform a rotation in $\mathbb{R}^3$ as shown in Figure 2.1 about the x-axis. The comparisons to the quaternion are primarily found in reference to the phenomenon of *gimbal lock* - the consequences of which are described in [34] - occurring when the composition of the matrices becomes rank deficient. Another notable consideration is the amount of operations required to determine the values in a rotation matrix and compose them. This quickly becomes more computationally demanding than quaternions, requiring lookup calls to sine and cosine functions in each timestep [36]. Of course, this method of rotation is still frequently used and in many applications can be considered sufficient for rotations in 3D space.

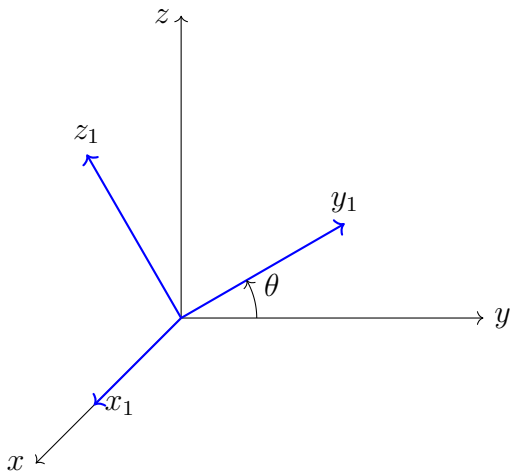

$$\begin{bmatrix} 1 & 0 & 0 \\ 0 & \cos(\theta) & -\sin(\theta) \\ 0 & \sin(\theta) & \cos(\theta) \end{bmatrix}$$

Figure 2.1: Matrix representation of rotation in $\mathbb{R}^3$

Rotations using quaternions may not be as visually intuitive, leading to the many resources aiming to provide a visual intuition for quaternions. The axis-angle formation is as visually representative as is necessary for this application. Quaternions are initialized with four values, or a vector and scalar part per Equation 2.2.

$$\mathbf{q} = \begin{bmatrix} \vec{q}_v \\ q_s \end{bmatrix} = \begin{bmatrix} q_1 \\ q_2 \\ q_3 \\ q_4 \end{bmatrix} \text{ such that } \mathbf{q} \in \mathbb{H} \tag{2.2}$$

Where the norm is $\|\boldsymbol{q}\| = \sqrt{q_1^2 + q_2^2 + q_3^2 + q_4^2} = \boldsymbol{q}^\intercal \boldsymbol{q}$. The placement of the scalar value above or below the vector part of the quaternion is largely arbitrary or a matter of opinion. In this work the scalar is placed below the vector component. The subscripts indicating the scalar and vector components are included for clarity as needed. The quaternion can be initialized using just a unit direction vector $\vec{n}$ and rotation angle θ to describe a rotation from a given frame of interest.

$$\mathbf{q} = \begin{bmatrix} \vec{n} \sin\left(\frac{\theta}{2}\right) \\ \cos\left(\frac{\theta}{2}\right) \end{bmatrix} \tag{2.3}$$

The factor of $\frac{1}{2}$ in the trigonometric function is a byproduct of the "double coverage" of SO(3). The benefit of this method of initialization is that the quaternion will have unit magnitude ($\|\boldsymbol{q}\| = 1$) by default. In fact, the only ordinary quaternions that properly represent rotations are unit quaternions. All ordinary quaternions simulated and presented in Chapter 5 have an imposed unit condition at each timestep.

Operations for ordinary quaternions are from [30], wherein the definition for ordinary quaternion multiplication is defined as in Equation 2.4. The operations for addition, subtraction and scaling for both ordinary and dual quaternions are element-wise operations and are intentionally omitted.

$$\mathbf{q}_1 \otimes \mathbf{q}_0 = \begin{bmatrix} q_1\vec{q}_0 + q_0\vec{q}_1 + \vec{q}_0 \times \vec{q}_1 \\ q_0 q_1 - \vec{q}_1 \cdot \vec{q}_0 \end{bmatrix} \tag{2.4}$$

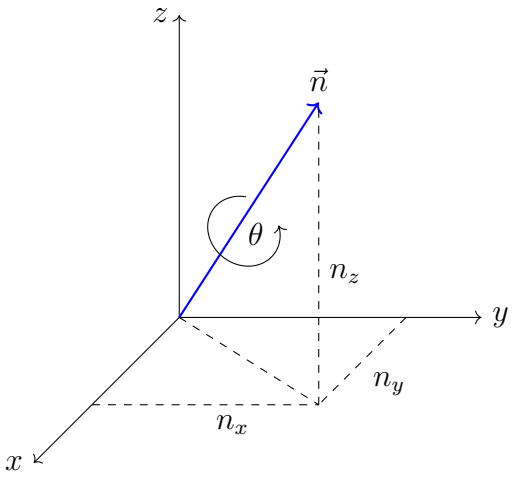

Figure 2.2: Axis-angle representation of rotation

Quaternion multiplication is used for the composition of successive rotations and the quaternion derivative. Note that all of the operations within the quaternion are algebraic and do not require calls to a trigonometric function, one of the tradeoffs when comparing the computational benefits of rotating with quaternions rather than with matrices.

$$\mathbf{q}^* = \begin{bmatrix} -\vec{q_v} \\ q_s \end{bmatrix} \tag{2.5}$$

The quaternion conjugate is simply the negation of the quaternion's vector part. Given the axis-angle visualization this holds some intuition as the same angle of rotation about the opposite axis would "undo" the initial rotation and mathematically speaking, return the identity quaternion $\mathbf{q}^*\mathbf{q} = \mathbf{q}_I = \mathbf{1}$. Finally, the dual quaternion cross product is defined in Equation 2.6, a necessary operation for calculating relative poses of frames for the dynamics presented in Chapter 3.

$$\mathbf{q}_1 \oslash \mathbf{q}_0 = \begin{bmatrix} q_1\vec{q_0} + q_0\vec{q_1} + \vec{q_1} \times \vec{q_0} \\ 0 \end{bmatrix} \tag{2.6}$$

2.3 Translation and Dual Quaternion Operations

For this application, dual quaternions are formulated as a pair of ordinary quaternions with the dual number ε separating the two, analogous to the complex numbers in the form $a + bi$. In contrast to the quaternion which is used to represent a rotation relative to another frame, a dual quaternion is considered to represent screw transformation, the translation and rotation about an axis in space. The expression for a dual quaternion and the dual number are formalized here for initialization.

$$\tilde{\mathbf{q}} = \mathbf{q} + \varepsilon\mathbf{d} \text{ where } \varepsilon^2 = 0 \text{ and } \varepsilon \neq 0 \tag{2.7}$$

Where $\mathbf{q}$ is initialized by use of Equation 2.3. The values $\mathbf{q}$ and $\mathbf{d}$ indicate the ordinary and dual parts of the dual quaternion. The dual number has other qualities beyond its unusual representation described in [25]. The formation of a dual quaternion is identical for the ordinary part given by Equation 2.3, but the dual component requires quaternion multiplication from Equation 2.4. To appropriately present the dual part, it is first necessary to clarify the difference between ordinary and pure quaternions. *Pure quaternions* have a zero-valued scalar part, and the vector part is the relevant vector in $\mathbb{R}^3$.

$$\vec{\omega} = \begin{bmatrix} \omega_x \\ \omega_y \\ \omega_z \end{bmatrix} \rightarrow \boldsymbol{\omega} = \begin{bmatrix} \omega_x \\ \omega_y \\ \omega_z \\ 0 \end{bmatrix}$$

It is with this convention that vectors such as the linear and angular velocity may be treated as pure quaternions, allowing the following definition for their respective dual part.

$$\mathbf{d} = \frac{1}{2}\mathbf{r}^{\mathcal{I}}_{B/I} \otimes \mathbf{q} = \frac{1}{2}\mathbf{q} \otimes \boldsymbol{r}^{\mathcal{B}}_{B/I} \tag{2.8}$$

$$\mathbf{d} = \frac{1}{2}\begin{bmatrix} \vec{r}^{\mathcal{I}}_{B/I} \\ 0 \end{bmatrix} \otimes \begin{bmatrix} \vec{q}_v \\ q_s \end{bmatrix} = \frac{1}{2}\begin{bmatrix} \vec{q}_v \\ q_s \end{bmatrix} \otimes \begin{bmatrix} \vec{r}^{\mathcal{B}}_{B/I} \\ 0 \end{bmatrix}$$

Where $\mathbf{r}^{\mathcal{B}}_{B/I}$ is a pure quaternion converted from the vector $\vec{r}^{\mathcal{I}}_{B/I}$, representing the distance between the origin of the inertial frame and the origin of the body frame, represented in the inertial frame. The expressions will yield the same result regardless of frame chosen, visually represented in Figure 2.3. The leftmost indicates that $\mathbf{q}$ occurs first, followed by the translation $\vec{r}$ in the relevant frame. Whether the rotation or the translation comes first is a matter of preference and application. For this work the translation will occur after the rotation.

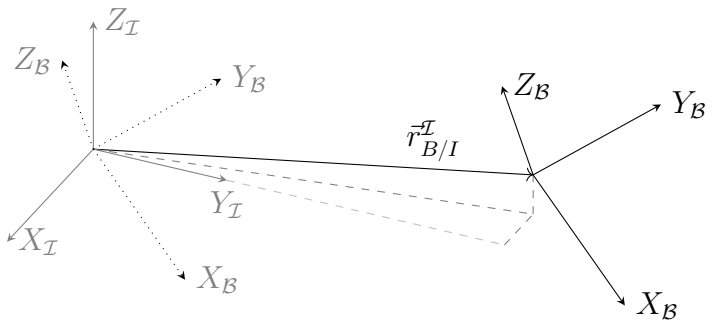

Figure 2.3: Reference frames as relative poses

Dual quaternion multiplication is defined by a series of quaternion multiplications. The convention for the dual quaternions is for the first entry to be the ordinary quaternion and the second entry the dual parts,

$$\tilde{\mathbf{q}}_1 \circledast \tilde{\mathbf{q}}_0 = \begin{bmatrix} \mathbf{q}_1 \\ \mathbf{d}_1 \end{bmatrix} \circledast \begin{bmatrix} \mathbf{q}_0 \\ \mathbf{d}_0 \end{bmatrix} = \begin{bmatrix} \mathbf{q}_1 \otimes \mathbf{q}_0 \\ \mathbf{q}_0 \otimes \mathbf{d}_1 + \mathbf{d}_0 \otimes \mathbf{q}_1 \end{bmatrix} \tag{2.9}$$

The conjugation operation and cross product operations follow as

$$\tilde{\mathbf{q}}^* = \begin{bmatrix} \boldsymbol{q}^* \\ \boldsymbol{d}^* \end{bmatrix} \tag{2.10}$$

$$\tilde{\mathbf{q}}_1 \oslash \tilde{\mathbf{q}}_0 = \begin{bmatrix} \mathbf{q}_1 \oslash \mathbf{q}_0 \\ \mathbf{q}_1 \oslash \mathbf{d}_0 + \mathbf{d}_1 \oslash \mathbf{q}_0 \end{bmatrix} \tag{2.11}$$

The symbol for quaternion cross product is the same for both ordinary and dual quaternions with the difference left to context. The dual quaternion norm, however, is not so trivial and two operations are defined for the dual quaternion that are not defined for the ordinary quaternion. The first of which is the dual quaternion circle product.

$$\tilde{\mathbf{q}}_0 \circ \tilde{\mathbf{q}}_1 = \boldsymbol{q}_0 \cdot \boldsymbol{q}_1 + \boldsymbol{d}_0 \cdot \boldsymbol{d}_1 \tag{2.12}$$

The result of the circle product is a scalar, which describes the dual quaternion norm by

$$\|\tilde{\mathbf{q}}\|^2 = \tilde{\mathbf{q}} \circ \tilde{\mathbf{q}} \tag{2.13}$$

The dual quaternion norm in Equation 2.13 is not the only method in which a norm can be defined in $\mathbb{H}$, but is used for its aid in later derivations, similar to the analysis performed in [13]. The final operation for the dual quaternion is the swap operation.

$$\tilde{\mathbf{q}}^s = \begin{bmatrix} \mathbf{d} \\ \mathbf{q} \end{bmatrix} \tag{2.14}$$

The swap operation is largely used to simplify the formulation of the dual inertia matrix and dual motor derivatives in Chapter 3.

Dual Error Quaternions

The ordinary error quaternion is not a wholly agreed-upon value in literature, and is usually defined as either the difference between the desired and the current quaternion $\mathbf{q}_E = \mathbf{q}_D - \mathbf{q}_C$ or as the relative rotation from the current attitude to the desired attitude. Its inclusion here is intended to appropriately preface the development of the relative kinetic equations.

$$\mathbf{q}_E \stackrel{\Delta}{=} \mathbf{q}^*_{B/I} \otimes \mathbf{q}_{G/I} = \mathbf{q}_{B/G} \tag{2.15}$$

The ordinary quaternion error can be used in the dynamics presented in Chapter 3 and is indeed used in the formulation of the control scheme. Note that in this formulation of the error quaternion the zero error condition is met at $\mathbf{q}_E = \begin{bmatrix} 0 & 0 & 0 & 1 \end{bmatrix}^\intercal = \mathbf{1}$. The dual quaternion case is effectively identical.

$$\tilde{\mathbf{q}}_E = \tilde{\mathbf{q}}^*_{B/I} \circledast \tilde{\mathbf{q}}_{G/I} = \tilde{\mathbf{q}}_{B/G} \tag{2.16}$$

2.4 Frames of Reference with Dual Quaternions

To preface discussion of dual quaternion dynamics, the natural question of reference frames must first be confronted. The relative rotation and position of one frame with respect to another is called the *pose* of a frame. The body frame is usually affixed to a satellite in some way convenient for design and with respect to some inertial frame. Note that as described in Equation 2.8 and shown visually in Figure 2.3, the rotation and translation may occur in any order.

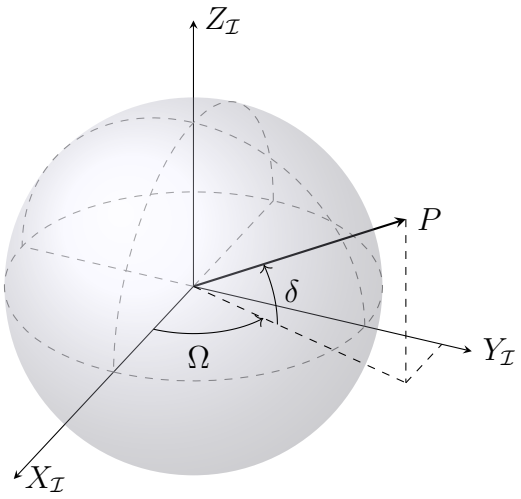

Figure 2.4: Geocentric equatorial frame definition

The inertial reference frame typically used for six degree-of-freedom simulation in LEO is the Geocentric Equatorial Frame (GEF) shown in Figure 2.4 The phrase 'inertial frame' is used equivalently to GEF in this work. The inertial frame is defined with the $X_{\mathcal{I}}$ axis aligned with the vernal equinox, the $Z_{\mathcal{I}}$ axis co-linear with the angular velocity of the earth, and with $(XY)_{\mathcal{I}}$ co-planar with earth's equatorial plane [9]. The GEF is not *strictly* inertial due to the influence of the sun and moon, among other effects. Changes significant enough to warrant correction require time-spans on the order of centuries. For this reason, the GEF is considered to be inertial for this system. Figure 2.4 shows the right ascension Ω and declination δ for a given point of interest along an orbit.

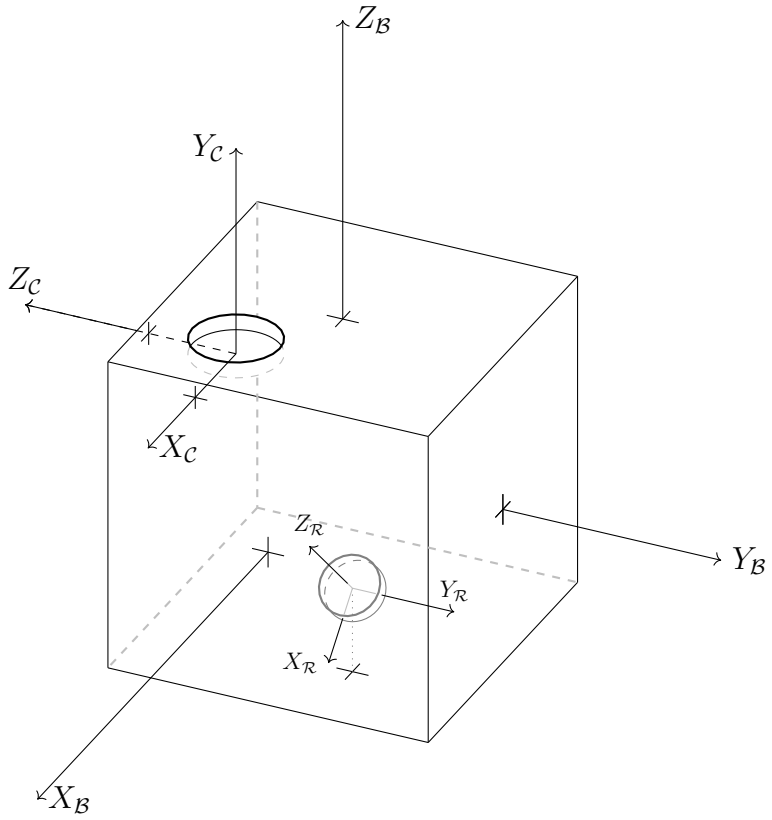

Figure 2.5: Body frame definition, with comms. ($\mathcal{C}$) frame and reaction wheel ($\mathcal{R}$) frames.

The body frame $\mathcal{B}$ is used to describe the pose of the satellite in space. In practice it's aligned in some convenient way for the operation of the spacecraft throughout the mission design. It may also act as its own point of reference for other frames, such as a camera frame, an antenna frame for some downlink boresight, or solar panel pointing. Figure 2.5 shows how these frames may be laid out relative to one another. The body frame is assumed be affixed in such a way that the inertia matrix encoding the distribution of mass on the spacecraft is diagonal. Ideally the distribution of mass would relate to some geometric "alignment" with relation to the structure of the spacecraft but this is neither required nor likely. For this case, the body frame forms an orthonormal basis aligned with the three principle moments of inertia. To express the relative orientation of a frame with respect to another, the ordinary quaternions can be used as follows to convert between frames.

$$\mathbf{r}^{\mathcal{Y}} = \mathbf{q}_{X/Y} \otimes \mathbf{r}^{\mathcal{X}} \otimes \mathbf{q}^{*}_{X/Y} \tag{2.17}$$

The equivalent frame conversion for the complete pose is calculated with a dual quaternion. In this calculation the offset generated by the relative position of the frame introduces a cross product term to the result, a manifestation of the transport theorem. Representing some given dual quaternion by $\tilde{\alpha}$ the transformation follows

$$\tilde{\alpha}^{\mathcal{Y}} = \tilde{\mathbf{q}}_{X/Y} \circledast \tilde{\alpha}^{\mathcal{X}} \circledast \tilde{\mathbf{q}}^{*}_{X/Y} = \begin{bmatrix} \boldsymbol{q}^{\mathcal{Y}}_{\alpha} \\ \boldsymbol{d}^{\mathcal{Y}}_{\alpha} - \boldsymbol{q}^{\mathcal{Y}}_{\alpha} \oslash \boldsymbol{r}^{\mathcal{Y}}_{X/Y} \end{bmatrix} \tag{2.18}$$

In the case where the $\mathcal{X}$ frame is desired with respect to $\mathcal{Y}$ the process is identical save for the flipped sign in the dual part. Given that $\tilde{\alpha}$ is formed from pure quaternions, the quaternion cross product reduces to the ordinary cartesian cross product. Therefore the changing of the sign can also be taken as 'flipping' the cross product, an intuitive result for moments and other rotational effects presented by an offset reference frame.

Chapter 3

SYSTEM DYNAMICS AND MODEL DEVELOPMENT

3.1 Dual Quaternion Dynamics

For the ordinary and the dual quaternions, the relevant kinematics and kinetics are derived here as is applicable to rendezvous. The pose of a spacecraft can be described completely with a quaternion and a position vector, requiring only seven floating point values. Of course, the quaternion is initialized using calls to sine and cosine upon initialization as shown in Equation 2.3. This cost occurs only when initializing the ordinary quaternion, and the call does not need to be made at each step of a simulation unlike rotation matrices. The computational benefit of dual quaternions is the ability to propagate the pose of the spacecraft with fewer floating point values, with calls to sine and cosine only upon initialization.

3.1.1 General Quaternion Kinematics

In general, controlling the angular and linear velocity of a spacecraft is an imperative part of any given mission design. The motivation for what/how it is controlled comes from various sources. Examples could include maximizing sun exposure to solar panels, improving pointing accuracy for a camera, or permitting clean data transmission to a ground station. The quaternion derivative is used to model the rotational dynamics.

$$\dot{\mathbf{q}}_{B/I} = \frac{1}{2}\mathbf{q}_{B/I} \otimes \boldsymbol{\omega}^{\mathcal{B}}_{B/I} = \frac{1}{2}\boldsymbol{\omega}^{\mathcal{I}}_{B/I} \otimes \mathbf{q}_{B/I} \tag{3.1}$$

The derivative of a quaternion is given by Equation 3.1 [9, 30, 29]. Using this equation informs the derivative of the dual quaternion, which is derived following the procedure in [29] with the addition of Equation 2.18.

$$\dot{\tilde{\mathbf{q}}}_{B/I} = \frac{d}{dt}\begin{bmatrix} \mathbf{q}_{B/I} \\ \frac{1}{2}\mathbf{r}^{\mathcal{I}}_{B/I} \otimes \mathbf{q}_{B/I} \end{bmatrix} = \frac{1}{2}\begin{bmatrix} \mathbf{q}_{B/I} \otimes \boldsymbol{\omega}^{\mathcal{B}}_{B/I} \\ \frac{d}{dt}\left(\mathbf{r}^{\mathcal{I}}_{B/I} \otimes \mathbf{q}_{B/I}\right) \end{bmatrix}$$

Starting then with the derivative of the dual quaternion and using the relationship shown in Equation 2.18 as $\mathbf{v}^{\mathcal{I}}_{B/I} = \mathbf{q}_{B/I} \otimes \mathbf{v}^{\mathcal{B}}_{B/I} \otimes \mathbf{q}^{*}_{B/I}$, conjugate both sides to form the equation $\mathbf{v}^{\mathcal{I}}_{B/I} \otimes \mathbf{q}_{B/I} = \mathbf{q}_{B/I} \otimes \mathbf{v}^{\mathcal{B}}_{B/I}$. The derivative of the dual part can then be written as:

$$\begin{aligned}
\frac{d}{dt}\left(\mathbf{r}^{\mathcal{I}}_{B/I} \otimes \mathbf{q}_{B/I}\right) &= \left(\mathbf{r}^{\mathcal{I}}_{B/I} \otimes \dot{\mathbf{q}}_{B/I}\right) + \left(\dot{\mathbf{r}}^{\mathcal{I}}_{B/I} \otimes \mathbf{q}_{B/I}\right) \\
&= \left(\mathbf{r}^{\mathcal{I}}_{B/I} \otimes \left(\frac{1}{2}\mathbf{q}_{B/I} \otimes \boldsymbol{\omega}^{\mathcal{B}}_{B/I}\right)\right) + \left(\dot{\mathbf{r}}^{\mathcal{I}}_{B/I} \otimes \mathbf{q}_{B/I}\right) \\
&= \frac{1}{2}\left(\mathbf{r}^{\mathcal{I}}_{B/I} \otimes \left(\mathbf{q}_{B/I} \otimes \boldsymbol{\omega}^{\mathcal{B}}_{B/I}\right)\right) + \left(\mathbf{v}^{\mathcal{I}}_{B/I} \otimes \mathbf{q}_{B/I}\right) \\
&= \frac{1}{2}\left(\mathbf{r}^{\mathcal{I}}_{B/I} \otimes \mathbf{q}_{B/I} \otimes \boldsymbol{\omega}^{\mathcal{B}}_{B/I}\right) + \mathbf{q}_{B/I} \otimes \mathbf{v}^{\mathcal{B}}_{B/I} \\
\dot{\tilde{\mathbf{q}}}_{B/I} &= \frac{1}{2}\begin{bmatrix} \mathbf{q}_{B/I} \otimes \boldsymbol{\omega}^{\mathcal{B}}_{B/I} \\ \frac{1}{2}\left(\mathbf{r}^{\mathcal{I}}_{B/I} \otimes \mathbf{q}_{B/I}\right) \otimes \boldsymbol{\omega}^{\mathcal{B}}_{B/I} + \mathbf{q}_{B/I} \otimes \mathbf{v}^{\mathcal{B}}_{B/I} \end{bmatrix}
\end{aligned}$$

Recognizing the above to be in the form of Equation 2.9, the derivative of the dual quaternion is concluded to be

$$\dot{\tilde{\mathbf{q}}}_{B/I} = \frac{1}{2}\tilde{\mathbf{q}}_{B/I} \circledast \tilde{\boldsymbol{\omega}}^{\mathcal{B}}_{B/I} = \frac{1}{2}\tilde{\boldsymbol{\omega}}^{\mathcal{I}}_{B/I} \circledast \tilde{\mathbf{q}}_{B/I} \tag{3.2}$$

This may also be applied to the dual error quaternion as $\dot{\tilde{\mathbf{q}}}_{E} = \frac{1}{2}\tilde{\mathbf{q}}_{E} \circledast \tilde{\boldsymbol{\omega}}_{E}$. The value $\tilde{\boldsymbol{\omega}}^{\mathcal{B}}_{B/I}$ is the dual quaternion formed from the linear and angular velocities in the body frame converted to pure quaternions, called the dual motor or dual velocity. Initializing the dual velocity is done as in Equation 3.3.

$$\tilde{\boldsymbol{\omega}}^{\mathcal{B}}_{B/I} = \boldsymbol{\omega}^{\mathcal{B}}_{B/I} + \varepsilon \mathbf{v}^{\mathcal{B}}_{B/I} \tag{3.3}$$

The transformations between reference frames that share an origin may be performed using ordinary quaternions and the same is true of the pose with dual quaternions. For the ordinary quaternion this extends to derivatives as well. However the rate of change in pose between two frames is typically accounted for using the classical *transport theorem*. The equivalent under a dual quaternion transformation is given in Equation 3.4 for the derivative of some dual quaternion $\tilde{\boldsymbol{\alpha}}$.

$$\dot{\tilde{\boldsymbol{\alpha}}}^{\mathcal{X}} = \tilde{\mathbf{q}}^{*}_{X/Y} \circledast \left(\dot{\tilde{\boldsymbol{\alpha}}}^{\mathcal{Y}} + \tilde{\boldsymbol{\omega}}^{\mathcal{Y}}_{Y/X} \oslash \tilde{\boldsymbol{\alpha}}^{\mathcal{Y}} \right) \circledast \tilde{\mathbf{q}}_{X/Y} \tag{3.4}$$

The result of which has the rotation of the frame $\mathcal{Y}$ with respect to $\mathcal{X}$, but can easily be negated and flipped if the measurement with respect to the $\mathcal{Y}$ frame is more efficient or practical. This formulation is the equivalent form of the transport theorem with respect to dual quaternions. The relative position of one frame with respect to another can be pulled directly from the dual quaternion as follows.

$$\boldsymbol{d} = \frac{1}{2}\boldsymbol{r}^{\mathcal{Y}}_{X/Y} \otimes \mathbf{q}_{X/Y} \rightarrow \boldsymbol{r}^{\mathcal{Y}}_{X/Y} = 2\boldsymbol{d} \otimes \mathbf{q}^{*}_{X/Y} \tag{3.5}$$

With the values above, the state of the satellite can be extracted from the dual quaternion by Equation 3.5 and by its respective quaternion $\mathbf{q}_{B/I}$.

3.1.2 General Quaternion Kinetics

The forces that act on a spacecraft depend on the gravitational parameter of the primary body, its atmosphere, multi-body effects, the geometry of the spacecraft, or even the incidence of light that the spacecraft receives, to name a few. The inertia matrix [**J**] is well-described in references such as [32, 31, 9] and the development thereof is not discussed in detail and is assumed to be diagonal. This analysis starts with the dual momentum, defined similarly to [13], in a general format.

$$\mathcal{H} = m\boldsymbol{v} + \varepsilon(\mathcal{J}\boldsymbol{\omega}) \tag{3.6}$$

Where the value $\boldsymbol{J}$ is the inertia matrix as is applicable to a pure quaternion, i.e. $\text{diag}(J_x, J_y, J_z, 1)$. The inertia matrix for the rigid body dynamics can be generalized to the dual quaternion formulation by the block-diagonal dual inertia matrix $\mathcal{J}$.

$$\mathcal{J} = \begin{bmatrix} m\boldsymbol{I}_{3\times3} & 0 & 0 & 0 \\ 0 & 1 & 0 & 0 \\ 0 & 0 & [\boldsymbol{J}] & 0 \\ 0 & 0 & 0 & 1 \end{bmatrix} \in \mathbb{R}^{8\times8} \tag{3.7}$$

The formulation of the dual momentum is contrary to the previous pattern wherein the 'rotational' effects are relegated to the ordinary quaternion. This choice of $\mathcal{J}$ requires a swap operation from Equation 2.14 in application but with this formulation the dual inertia matrix is symmetric and diagonal. As is classically the case, the change in dual momentum in an inertial frame is equal to the forces acting on the inertial frame. Applying Equation 3.4 to the inertial case, the change in the dual momentum and forces can be calculated. The formulation of this is shown in Equations 3.8 and 3.9. A visualization of the dual momentum is shown in Figure 3.1, where the torque $\vec{\tau}_B$ is independent of force $\vec{f}_A$.

$$\dot{\mathcal{H}}^{\mathcal{I}}_{B/I} = \boldsymbol{f}^{\mathcal{I}} \tag{3.8}$$

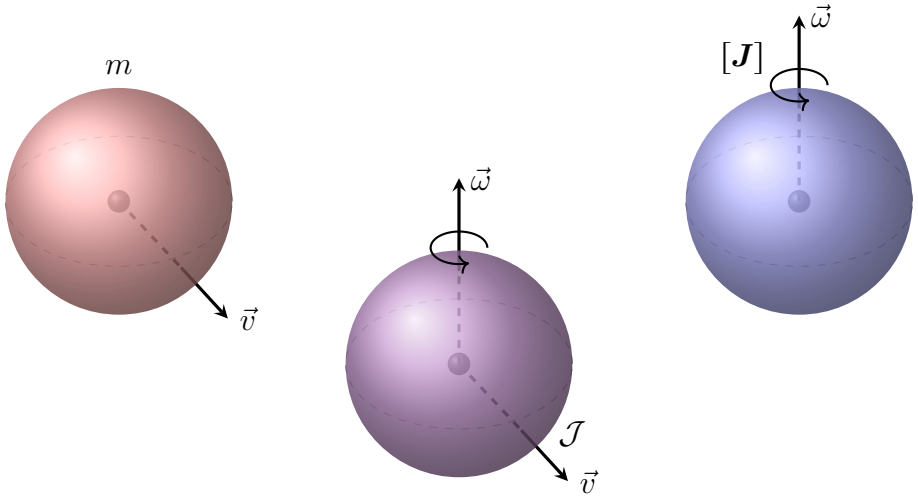

Figure 3.1: Dual Momentum $\mathcal{H}$ as a combination of linear and angular velocities.

$$\dot{\mathcal{H}}^{\mathcal{B}}_{B/I} + \tilde{\boldsymbol{\omega}}^{\mathcal{B}}_{B/I} \oslash \mathcal{H}^{\mathcal{B}}_{B/I} = \tilde{\boldsymbol{f}}^{\mathcal{B}} \tag{3.9}$$

Where the force $\tilde{\boldsymbol{f}}^{\mathcal{B}} = \vec{f}^{\mathcal{B}} + \varepsilon\vec{\tau}^{\mathcal{B}}$. This is another byproduct of the choice in $\mathcal{J}$ where a diagonal matrix formation is not only simpler, it also doesn't require the need for a dual operator as described in [5]. There are anti-symmetric versions of $\mathcal{J}$ too, but they are not used in this work. The matrix $\mathcal{J}$ is used to relate the dual momentum to the *swapped* dual velocity due to the definition in Equation 3.6

$$\dot{\boldsymbol{\mathcal{H}}}^{\mathcal{B}}_{B/I} = \mathcal{J}_B \left(\dot{\tilde{\boldsymbol{\omega}}}^{\mathcal{B}}_{B/I}\right)^s \tag{3.10}$$

Substituting Equation 3.10 and 3.8 into Equation 3.9, the rigid body equation used for control law development and simulation is expressed fully. The result can be swapped once again for propagation.

$$\boxed{\left(\dot{\tilde{\boldsymbol{\omega}}}^{\mathcal{B}}_{B/I}\right)^s = \mathcal{J}_B^{-1}\left(\tilde{\boldsymbol{f}}^{\mathcal{B}} - \tilde{\boldsymbol{\omega}}^{\mathcal{B}}_{B/I} \oslash \left(\mathcal{J}_B \left(\tilde{\boldsymbol{\omega}}^{\mathcal{B}}_{B/I}\right)^s\right)\right)} \tag{3.11}$$

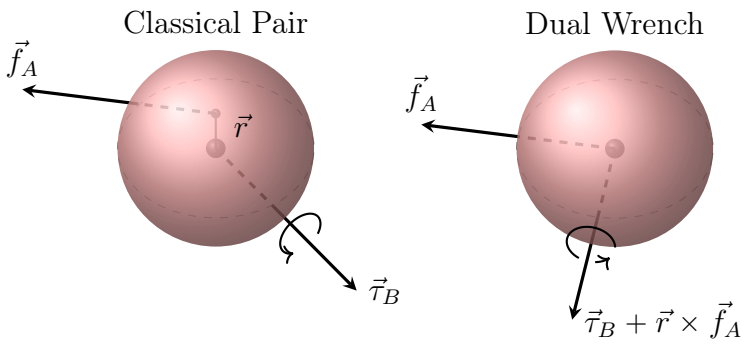

Figure 3.2: Dual Wrench $\tilde{\boldsymbol{f}}$ as a combination of forces and moments on a body.

The formulation in Equation 3.11 works for the mapping of a pose in space for a single spacecraft, but does not account for the relative motion between two frames. The relative velocity of the $\mathcal{B}$ frame with respect to $\mathcal{G}$ is derived as follows.

$$
\begin{aligned}
\left(\tilde{\boldsymbol{\omega}}^{\mathcal{B}}_{B/G}\right)^s &= \left(\tilde{\boldsymbol{\omega}}^{\mathcal{B}}_{B/I}\right)^s - \left(\tilde{\boldsymbol{\omega}}^{\mathcal{B}}_{G/I}\right)^s \\
\left(\dot{\tilde{\boldsymbol{\omega}}}^{\mathcal{B}}_{B/G}\right)^s &= \left(\dot{\tilde{\boldsymbol{\omega}}}^{\mathcal{B}}_{B/I}\right)^s - \left(\dot{\tilde{\boldsymbol{\omega}}}^{\mathcal{B}}_{G/I}\right)^s \\
\left(\dot{\tilde{\boldsymbol{\omega}}}^{\mathcal{B}}_{B/G}\right)^s &= \mathcal{J}_B^{-1}\left(\boldsymbol{f}^{\mathcal{B}} - \tilde{\boldsymbol{\omega}}^{\mathcal{B}}_{B/I} \oslash \left(\mathcal{J}_B\left(\tilde{\boldsymbol{\omega}}^{\mathcal{B}}_{B/I}\right)^s\right)\right) - \left(\dot{\tilde{\boldsymbol{\omega}}}^{\mathcal{B}}_{G/I}\right)^s \\
\left(\dot{\tilde{\boldsymbol{\omega}}}^{\mathcal{B}}_{B/G}\right)^s &= \mathcal{J}_B^{-1}\left(\boldsymbol{f}^{\mathcal{B}} - \tilde{\boldsymbol{\omega}}^{\mathcal{B}}_{B/I} \oslash \left(\mathcal{J}_B\left(\tilde{\boldsymbol{\omega}}^{\mathcal{B}}_{B/I}\right)^s\right)\right) - \left(\tilde{\mathbf{q}}^*_{B/G} \circledast \left(\dot{\tilde{\boldsymbol{\omega}}}^{\mathcal{G}}_{G/I} + \tilde{\boldsymbol{\omega}}^{\mathcal{G}}_{G/I} \oslash \tilde{\boldsymbol{\omega}}^{\mathcal{G}}_{B/G}\right) \circledast \tilde{\mathbf{q}}_{B/G}\right)^s
\end{aligned}
$$

The final equality is presented in different ways depending on the intended application, but they remain the same relationship. These differences present themselves in [3, 13], where the relative motion is modeled by the following two equations, with the dual 'coriolar' effect converted into the $\mathcal{B}$ frame.

$$
\left(\dot{\tilde{\boldsymbol{\omega}}}^{\mathcal{B}}_{B/G}\right)^s = \mathcal{J}_B^{-1}\left(\boldsymbol{f}^{\mathcal{B}} - \tilde{\boldsymbol{\omega}}^{\mathcal{B}}_{B/I} \oslash \left(\mathcal{J}_B\left(\tilde{\boldsymbol{\omega}}^{\mathcal{B}}_{B/I}\right)^s\right)\right) - \left(\tilde{\mathbf{q}}^*_{B/G} \circledast \dot{\tilde{\boldsymbol{\omega}}}^{\mathcal{G}}_{G/I} \circledast \tilde{\mathbf{q}}_{B/G}\right)^s - \left(\tilde{\boldsymbol{\omega}}^{\mathcal{B}}_{B/I} \oslash \tilde{\boldsymbol{\omega}}^{\mathcal{B}}_{G/I}\right)^s \tag{3.12}
$$

The relationship in Equation 3.12 describes the relative the pose of $\mathcal{B}$ with respect to $\mathcal{G}$ under forces from the space environment. However, this is under the assumption that the pose of the goal frame is either known or measurable. In reality $\mathcal{G}$ is a pose in space defined

either by mission requirements or *in relation* to the $\mathcal{B}$ frame. This is to say that it may not be associated with a physical object in space. The pose relating $\mathcal{B}$ to some frame attached to a physical target $\mathcal{T}$ may be used to formulate $\mathcal{G}$. This methodology is the same used to determine the pose between two multi-joint robotic arms with dual quaternions. The dynamics in the simulation are the same as Equation. 3.12, but to express the proximity operations case the terms are converted into values that could be reasonably measured in $\mathcal{B}$ from $\mathcal{T}$. This leaves the pose of $\mathcal{G}$ as a matter of mission specifications.

$$\begin{aligned}\tilde{\mathbf{q}}_{B/G} &= \tilde{\mathbf{q}}^*_{G/I} \circledast \tilde{\mathbf{q}}_{B/I} \\ \tilde{\mathbf{q}}_{B/G} &= \tilde{\mathbf{q}}^*_{G/T} \circledast \tilde{\mathbf{q}}_{B/T} \\ \tilde{\mathbf{q}}_{E} &= \tilde{\mathbf{q}}^*_{G/T} \circledast \tilde{\mathbf{q}}_{B/T}\end{aligned}$$

The error dual quaternion $\tilde{\mathbf{q}}_{B/G}$ is defined by the following, as introduced in Section 2.3, the purpose of which is to get the relative pose of the $\mathcal{B}$ and $\mathcal{G}$ frame with respect to a more easily accessible frame. The measurement between the target and the body can be done with the inclusion of camera or some other visual sensor and many recent options have used computer vision techniques for 6DOF pose estimation. This relationship can then be substituted into Equation 3.12.

$$\left(\dot{\tilde{\boldsymbol{\omega}}}^{\mathcal{B}}_{B/G}\right)^s = \mathcal{J}_B^{-1}\left(\tilde{\boldsymbol{f}}^{\mathcal{B}} - \tilde{\boldsymbol{\omega}}^{\mathcal{B}}_{B/I} \oslash \left(\mathcal{J}_B\left(\tilde{\boldsymbol{\omega}}^{\mathcal{B}}_{B/I}\right)^s\right)\right) - \left(\tilde{\mathbf{q}}^*_E \circledast \dot{\tilde{\boldsymbol{\omega}}}^{\mathcal{G}}_{G/I} \circledast \tilde{\mathbf{q}}_E\right)^s - \left(\tilde{\boldsymbol{\omega}}^{\mathcal{B}}_{B/I} \oslash \tilde{\boldsymbol{\omega}}^{\mathcal{B}}_{G/I}\right)^s$$

This provides the pose as a composition of two quaternions, but does not yet account for the dual velocity motor. To calculate the $\left(\tilde{\boldsymbol{\omega}}^{\mathcal{B}}_{G/I}\right)^s$ term the following is presented

$$\begin{aligned}\tilde{\boldsymbol{\omega}}^{\mathcal{B}}_{G/I} &= \tilde{\boldsymbol{\omega}}^{\mathcal{B}}_{B/I} - \tilde{\boldsymbol{\omega}}^{\mathcal{B}}_{B/G} \\ \tilde{\boldsymbol{\omega}}^{\mathcal{B}}_{B/I} \oslash \tilde{\boldsymbol{\omega}}^{\mathcal{B}}_{G/I} &= \cancel{\tilde{\boldsymbol{\omega}}^{\mathcal{B}}_{B/I} \oslash \tilde{\boldsymbol{\omega}}^{\mathcal{B}}_{B/I}}^{\to 0} - \tilde{\boldsymbol{\omega}}^{\mathcal{B}}_{B/I} \oslash \tilde{\boldsymbol{\omega}}^{\mathcal{B}}_{B/G} \\ \tilde{\boldsymbol{\omega}}^{\mathcal{B}}_{B/I} \oslash \tilde{\boldsymbol{\omega}}^{\mathcal{B}}_{G/I} &= -\tilde{\boldsymbol{\omega}}^{\mathcal{B}}_{B/I} \oslash \tilde{\boldsymbol{\omega}}^{\mathcal{B}}_{B/G} \\ \tilde{\boldsymbol{\omega}}^{\mathcal{B}}_{B/I} \oslash \tilde{\boldsymbol{\omega}}^{\mathcal{B}}_{G/I} &= -\tilde{\boldsymbol{\omega}}^{\mathcal{B}}_{B/I} \oslash (\tilde{\boldsymbol{\omega}}^{\mathcal{B}}_{B/T} - \tilde{\boldsymbol{\omega}}^{\mathcal{B}}_{G/T})\end{aligned}$$

Once again back-substituting this result into Equation 3.12, the relative dynamics between the body and the goal frame can be described equivalently by measurements of the target frame.

$$\left(\dot{\tilde{\boldsymbol{\omega}}}^{\mathcal{B}}_{B/G}\right)^{s} = \mathcal{J}_B^{-1}\left(\tilde{\boldsymbol{f}}^{\mathcal{B}} - \tilde{\boldsymbol{\omega}}^{\mathcal{B}}_{B/I} \oslash \left(\mathcal{J}_B\left(\tilde{\boldsymbol{\omega}}^{\mathcal{B}}_{B/I}\right)^{s}\right) - \left(\tilde{\mathbf{q}}^{*}_{E}\dot{\tilde{\boldsymbol{\omega}}}^{\mathcal{G}}_{G/I}\tilde{\mathbf{q}}_{E}\right)^{s} + \left(\tilde{\boldsymbol{\omega}}^{\mathcal{B}}_{B/I} \oslash \left(\tilde{\boldsymbol{\omega}}^{\mathcal{B}}_{B/T} - \tilde{\boldsymbol{\omega}}^{\mathcal{B}}_{G/T}\right)\right)^{s}\right. \tag{3.13}$$

The values in Equation 3.13 are either considered to be measurable quantities with a sensor or defined as a parameter of the mission. The exception is the term $\dot{\tilde{\boldsymbol{\omega}}}^{\mathcal{G}}_{G/I}$. This value can be calculated by $\dot{\tilde{\boldsymbol{\omega}}}^{\mathcal{G}}_{G/T} + \dot{\tilde{\boldsymbol{\omega}}}^{\mathcal{G}}_{T/I} = \dot{\tilde{\boldsymbol{\omega}}}^{\mathcal{G}}_{G/I}$ by using Equation 3.13 for the $\dot{\tilde{\boldsymbol{\omega}}}^{\mathcal{G}}_{G/T}$. Under the condition that the target and goal frame are coincident, i.e. $\tilde{\mathbf{q}}_{G/I} = \tilde{\mathbf{q}}_{T/I}$, then $\tilde{\mathbf{q}}_{B/G} \rightarrow \tilde{\mathbf{q}}_{B/T}$ indicating that the desired pose is exactly where the target would be. This is the rendezvous problem as a specific case of proximity operations. The rest of the work will assume that the poses relative to $\mathcal{I}$ for both $\mathcal{T}$ and $\mathcal{G}$ are coincident.

3.2 Orbital Perturbations and Test Conditions

The primary force acting on a satellite is gravity, calculated as follows and used in the simulation to propagate the path of the spacecraft forward.

$$\tilde{\boldsymbol{f}}_{Grav} = -\frac{\mu_{earth}}{r^2}\hat{u}_r \tag{3.14}$$

During simulation of the satellite attempting rendezvous, the orbit chosen will have effects on the motion of the spacecraft in an orbit defined by Equation 3.14. In LEO there are a barrage of small forces and torques acting on the body at any given time. The gravity gradient torques, the drag wrench, and J_2 effects are described here. This provides disturbances in both the ordinary and the dual part of the pose dual quaternion.

Oblateness of the Earth, J_2 Effects

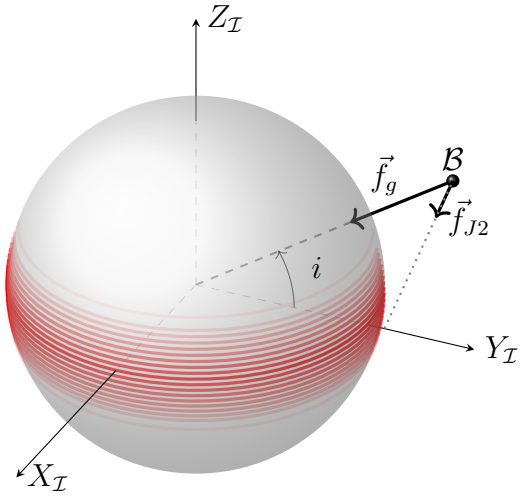

Figure 3.3: J_2 effects on a satellite in orbit.

The value J_2 is one of many constants defined by spherical zonal harmonics, a model of the Earth's oblateness. However for the satellite in LEO the effects are going to be dominated by the first harmonic J_2, caused by the additional mass concentration near the equator, shown in red in Figure 3.3. These equations are modeled as a force in the $\mathcal{B}$ frame in [9, 32, 31] for example.

$$\frac{1}{m}\vec{f}_{J_2} = \frac{3}{2}\frac{J_2\mu R_{earth}^2}{r^4}\begin{bmatrix} \frac{x}{r}\left(5\frac{z^2}{r^2}-1\right) \\ \frac{y}{r}\left(5\frac{z^2}{r^2}-1\right) \\ \frac{z}{r}\left(5\frac{z^2}{r^2}-3\right) \end{bmatrix} \tag{3.15}$$

The effects of higher harmonics are truncated in this case, as they will not affect the spacecraft throughout the timescales of rendezvous. The J_2 effect comes mostly as a byproduct of the equator having a larger diameter than the polar diameter of the planet. The dual force is then an ordinary quaternion and takes the form $\tilde{\boldsymbol{f}}_{J_2} = \boldsymbol{f}_{J_2} + \varepsilon\mathbf{0}$

Aerodynamic Drag

In LEO the aerodynamic effects applied to a satellite are small, but cannot be ignored over mission timespans, especially in LEO, where aerodynamic drag in LEO is an unavoidable consequence of the remnant atmosphere at high altitude. The model for the aerodynamic drag in space and in general is as follows [4, 9].

$$\vec{f}_{aero} = -\frac{1}{2} m \rho B \|v_{B/atm}\|^2 \hat{v}_{B/atm} \tag{3.16}$$

Where $B = \frac{C_D A}{m}$ is the ballistic coefficient. The drag forces acting on the satellite are described about the center of mass in [9, 32, 22]. However, a given satellite may have its aerodynamic center ($\boldsymbol{r}_{ac/B}$) offset from its center of mass, inducing a torque [4]. Resolving this phenomenon is a convenient use of dual quaternions, where the aerodynamic wrench can be cleanly defined.

$$\tilde{\boldsymbol{f}} = \boldsymbol{f}_{aero} + \varepsilon(\boldsymbol{r}_{ac/B} \oslash \boldsymbol{f}_{aero}) \tag{3.17}$$

The effect of an aerodynamic moment on the satellite about the center of mass is omitted in [9, 22, 32], but the order of magnitude of such torques are similar in magnitude to other perturbations. The contribution of this work considers an area frame with respect to the center of mass where the aerodynamic effects are applied. The drag coefficient is dependent on the ordinary quaternion, i.e. $C_D = f(q_{B/atm})$ and $A_\perp = f(q_{B/I})$ but in an effort to generalize the aerodynamic wrench simply, a pose-independent constant drag coefficient is considered. The calculation of the drag coefficient and ballistic coefficient is no small undertaking in general, requiring a good model of the orbit and atmospheric conditions.

To capture the effects of the aerodynamic force on the satellite the relative motion of the atmosphere is taken to match the rotational speed of the Earth $\vec{\omega}_{earth}$. The rotational speed locally for the satellite can then be described by $\vec{v}_{atm/I} = \vec{\omega}_{earth} \times \vec{r}^{\mathcal{I}}_{B/I}$. The relative motion is then given by $\vec{v}_{atm/B} = \vec{\omega}_{earth} \times \vec{r}^{\mathcal{I}}_{B/I} - \vec{v}_{B/I}$.

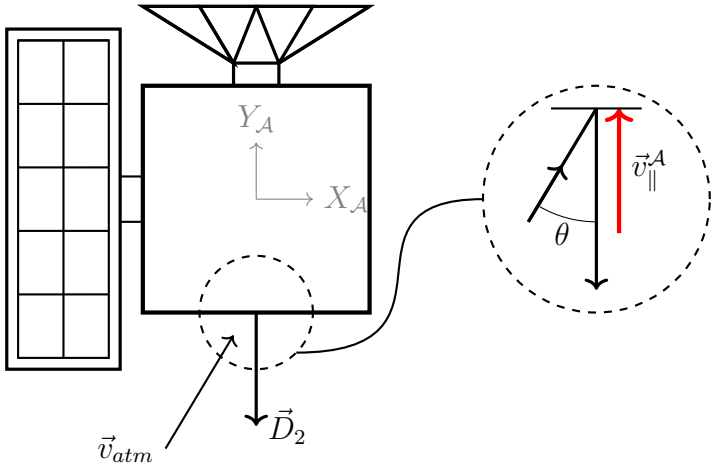

Figure 3.4: Surface area considerations for $\mathcal{A}$ frame and drag calculations.

Let there be a set of vectors with directions associated with the normal vector of each relevant surface on the satellite and with magnitude equal to the area of the given surface $\mathcal{D} \in \left\{C_{D_1}\vec{A}_1, -C_{D_1}\vec{A}_1, \cdots, C_{D_n}\vec{A}_n, -C_{D_n}\vec{A}_n\right\}$. These vectors do not have to be orthogonal and are simply a collection of oriented areas, expressed in some convenient area frame $\mathcal{A}$. Each vector magnitude correlates with the area of some surface multiplied by its respective drag coefficient.

$$\vec{D}_i = C_{Di}\vec{A}_i \in \mathcal{D}$$
$$\vec{f}_{aero}^{\mathcal{A}} = -\frac{1}{2}\rho\vec{v}_{\parallel}^{\mathcal{A}}\sum_{i=1}^{n}\left(\vec{D}_i \cdot \vec{v}_{\parallel}^{\mathcal{A}}\right)$$
$$\boldsymbol{f}_{aero}^{\mathcal{B}} = \boldsymbol{q}_{A/B} \otimes \boldsymbol{f}_{aero}^{\mathcal{A}} \otimes \boldsymbol{q}_{A/B}^{*}$$

Assuming then that each of the body axes has an associated normal vector/area pair and a drag coefficient, the drag of each individual face can be calculated as the dot product of the body normal vector with the parallel velocity $\vec{v}_{\parallel} = \vec{v}_{atm/I}^{\mathcal{B}} \cdot \vec{v}_{B/I}^{\mathcal{B}}$. Other faces may be added without loss of generality and for a straightforward application an orthogonal set of faces aligning with the positive and negative $\pm\hat{x}_B$, $\pm\hat{y}_B$, and $\pm\hat{z}_B$ may be used.

Then with the force defined about the aerodynamic center in the body frame, the dual drag can be defined using Equation 3.17

$$\tilde{\boldsymbol{f}}_{aero} = \begin{bmatrix} \boldsymbol{q}_{A/B} \otimes \boldsymbol{f}^{\mathcal{A}}_{aero} \otimes \boldsymbol{q}^{*}_{A/B} \\ \boldsymbol{r}_{ac/B} \oslash \left(\boldsymbol{q}_{A/B} \otimes \boldsymbol{f}^{\mathcal{A}}_{aero} \otimes \boldsymbol{q}^{*}_{A/B} \right) \end{bmatrix} \tag{3.18}$$

3.2.1 Gravity Gradient

The gravitational effects on a satellite will act throughout its body in a manner dependent on the distribution of its mass. While the assumption in this case is that the inertia matrix is diagonal, the differences between the principal values will have an effect on which given axis is most affected by the gravitational pull of the earth. The gravity gradient is presented plainly as a torque on the body from [9, 32].

$$\tilde{\boldsymbol{f}}_{GG} = \begin{bmatrix} r_y r_z (J_{Bz} - J_{By}) \\ r_x r_z (J_{Bx} - J_{Bz}) \\ r_x r_y (J_{By} - J_{Bx}) \\ 0 \end{bmatrix} \tag{3.19}$$

Where $\vec{r}^{\mathcal{I}}_{B/I} = [r_x \; r_y \; r_z]^\intercal$ is the position of the satellite with respect to the inertial frame. Note that in the case where the spacecraft is fully symmetric $J_{Bx} = J_{By} = J_{Bz}$ (i.e. a cube, sphere, etc.) the gravity gradient is zero.

3.2.2 Orbital Test Cases and Simulation Parameters

The rendezvous' simple case takes place in LEO directly above the equator, with classical orbital elements listed in Table 3.1. This is intended to mimic the most common type of satellite configuration. The second case is based on the 12U Maratus CubeSat under development at the University of Washington. Both cases are visualized in in Figures 3.5 and 3.6, and the baseline parameters used for the simulation of the orbit and all control parameters are in Table 3.2. The control gains are defined in Chapter 4.

Case	a	e	i	Ω	ω	θ
LEO	$R_{earth} + \rho$	0	0°	N/A	N/A	0°
Maratus	$R_{earth} + 600$km	0.003	56°	60°	N/A	0°

Table 3.1: Classical orbital elements for orbital cases

Term	**Value**
k_p	0.025
k_d	0.4
k_f	2
k_{CBF}	0.01
α	0.01
β	50
m_B	10 kg

Term	**Value**
$\vec{r}^{\mathcal{I}}_{B/G}$	[-50 -2 15] m
$\vec{v}^{\mathcal{I}}_{B/G}$	[1 -0.1 1.1] $\frac{\text{m}}{\text{s}}$
$\vec{\omega}^{\mathcal{I}}_{B/G}$	[0.01 -0.01 0.5236] $\frac{\text{rad}}{\text{s}}$
$\boldsymbol{q}_{B/I}$	[0.2315 0.4629 0.6944 0.5]
$\boldsymbol{q}_{G/I}$	[0 0 0 1]
J_B	$\begin{bmatrix} 2 & 0 & 0 \\ 0 & 1.1 & 0 \\ 0 & 0 & 0.5 \end{bmatrix}$ kg $\cdot$ m^2

Table 3.2: Baseline numerical simulation parameters

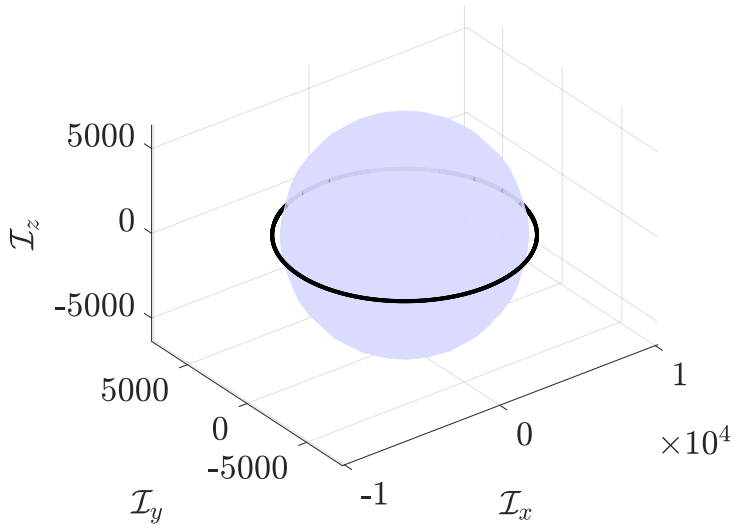

Figure 3.5: LEO orbit case

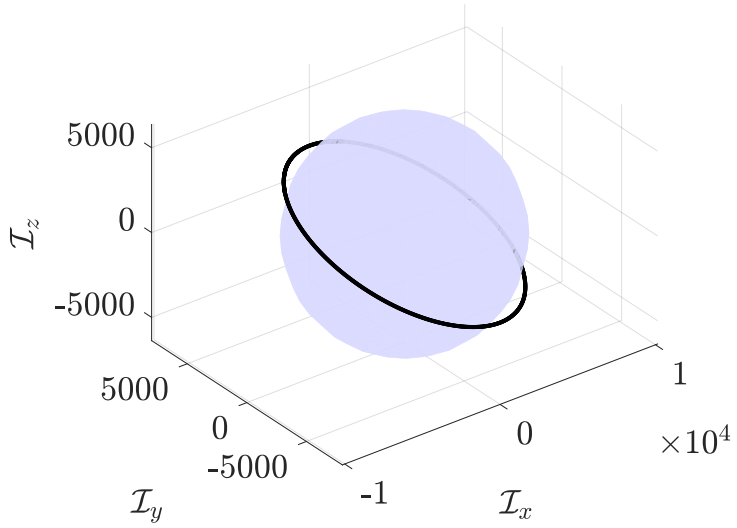

Figure 3.6: Maratus orbit case

Chapter 4
CONTROL LAW FORMULATION

The control method presented in this work for satellite rendezvous is a combination of two separate methods with the ordinary quaternion controlling the attitude via logarithmic control barrier functions and the entire dual quaternion used to align the $\mathcal{B}$ frame with the $\mathcal{G}$ frame. The controller is designed to force $\mathbf{q}_E \to \mathbf{1}$ and $\tilde{\boldsymbol{\omega}}^{\mathcal{B}}_{B/G} \to 0$ while avoiding particular attitudes in inertial space. The state for the control law includes the relative pose represented as dual quaternions, its associated dual velocity, and a filter state.

4.1 Dual Quaternion Feedback Control Methodology

The proposed controller is developed in steps, first as a proportional & derivative (PD) controller, then followed by an attitude-only controller. In both cases the relative motion between the frames is used to generate control wrenches. The use of dual quaternions cleanly combines these types of controllers, as the attitude only controller may be applied to ordinary part of the dual quaternion without difficulty and the relative pose between the two satellites may still use the ordinary part to correct errors in the relative position.

4.2 Dual PD Controller Formulation

The first component of the overall control design is in the form of a PD controller with matrices k_P and k_D as the control gains. This analysis is performed generally following the controller design methodology developed in [13] under the assumption that the relative motor of the goal frame is measurable. The controller for the simulation of relative motion is defined as

$$\boldsymbol{f}^{\mathcal{B}} = -k_p \mathrm{vec}(\tilde{\mathbf{q}}^*_{B/G}(\tilde{\mathbf{q}}^s_{B/G} - \tilde{\mathbf{1}}^s)) - k_d(\tilde{\boldsymbol{\omega}}^{\mathcal{B}}_{B/G})^s + \mathcal{J}_B(\tilde{\mathbf{q}}^*_{B/G}\dot{\tilde{\boldsymbol{\omega}}}^{\mathcal{G}}_{G/I}\tilde{\mathbf{q}}_{B/G})^s + \tilde{\boldsymbol{\omega}}^{\mathcal{B}}_{G/I} \oslash (\mathcal{J}_B(\tilde{\boldsymbol{\omega}}^{\mathcal{B}}_{G/I}))$$

The final terms of this controller come directly as a byproduct of the dynamics in Chapter 3 in Equation 3.12. Removing the relative terms for clarity, the controller can be presented as a PD controller with gains k_p and k_d

$$\boldsymbol{f}^{\mathcal{B}} = -k_p \text{vec}(\tilde{\mathbf{q}}^*_{B/G}(\tilde{\mathbf{q}}^s_{B/G} - \tilde{\mathbf{1}}^s)) - k_d(\tilde{\boldsymbol{\omega}}^{\mathcal{B}}_{B/G})^s \tag{4.1}$$

Where the terms k_p, k_d must be greater than or equal to zero. Other formations of this type of dual quaternion control system have been presented in [39]. This particular formation requires measurements of the dual motor, a difficult procedure in practice and not fully within the scope here. To resolve the measurement problem a filter is used to synthesize the measurement of $\tilde{\boldsymbol{\omega}}^{\mathcal{B}}_{B/G}$ as such

$$\dot{\tilde{\boldsymbol{x}}}_f = A\tilde{\boldsymbol{x}}_f + B\tilde{\mathbf{q}}_{B/G} \tag{4.2}$$

$$\tilde{\boldsymbol{z}} = CA\tilde{\boldsymbol{x}}_f + CB\tilde{\mathbf{q}}_{B/G} \tag{4.3}$$

The above forms come from [13, 14] and describe what is effectively a low-pass filter on $\tilde{\mathbf{q}}_{B/G}$, and is stable assuming that the matrices A, B, and C are a minimal realization of some positive real transfer function that satisfies $PA + A^\intercal P = -Q$ and $PB = C^\intercal$ where P, Q are positive definite symmetric matrices. Then Equation 4.1 becomes

$$\boldsymbol{f}^{\mathcal{B}} = -k_p \text{vec}(\tilde{\mathbf{q}}^*_{B/G}(\tilde{\mathbf{q}}^s_{B/G} - \tilde{\mathbf{1}}^s)) - 2\text{vec}(\tilde{\mathbf{q}}^*_{B/G}\tilde{\boldsymbol{z}}^s) \tag{4.4}$$

The variable $\tilde{\boldsymbol{z}}$ is the output of the filter defined in Equation 4.2. As was done to arrive at Equation 4.1, the relative terms are removed for clarity. In the context of the modified dynamics generated in Equation 3.13 the controller will still stabilize the pose of the body, as the underlying dynamics have not changed. The simulations and hardware tests performed in [13, 14, 31] set the matrices $A = k_f \boldsymbol{I}_{8\times 8}$ and $B = -k_f \boldsymbol{I}_{8\times 8}$, and $C = k_d$ by the KYP Lemma, and this formulation is maintained here.

4.2.1 Ordinary Quaternion Control Barrier Function

Constraints on the attitude of a satellite may come from various sources, and could be a way to ensure that some sensitive instrument does not get damaged or to satisfy mission requirements for example. For this application the assumption is that there is some restriction on the attitudes that the satellite may take. There are many ways to confront this issue and various methods have been tried such as successive convex optimization. The attitude constraints here are accounted for by the use of a control barrier function, described in two parts. The back-stepping method is applied to the satellite dynamics from [23, 21]. Then the development of a suitable Lyapunov function for the system based on [39] is completed.

4.3 Non-Linear Control via Back-stepping and Lyapunov Stability

Take a dynamic system in strict feedback form to be $\dot{x} = f_x(x, \beta)$ and $\dot{\beta} = f_u(x, u)$. As there is no direct means of control u in $f_x(x, \beta)$, formulating a controller is a matter of determining a *virtual control* β_{vc} in $f_x(x, \beta)$ that will affect $\dot{x}$. By defining an error state $z = \beta - \beta_{vc}$, a choice of u can be made to force $z \to 0$ and 'back-stepping' that effect to control $\dot{x}$, typically by equating it with the negative of the gradient of its respective Lyapunov function.

Following the above procedure generally with inspiration from [21] the systems are Equation 3.1 and Euler's rotation equations $J\dot{\vec{\omega}} = \vec{\tau} - \vec{\omega} \times (J\vec{\omega})$. The virtual control term then becomes $\boldsymbol{\omega}_{vc}$ and control vector $\vec{\tau}$. The development of the Lyapunov function for this application is performed in Section 4.3.1. To start $\dot{\boldsymbol{q}} = -\nabla V \to \dot{\boldsymbol{q}} = \frac{1}{2}\boldsymbol{q} \otimes \boldsymbol{\omega} \to \boldsymbol{\omega}_{vc} = -2\boldsymbol{q}^* \otimes \nabla V$. The back-stepping process is then as follows, starting with the definition of the error variable.

$$\boldsymbol{z} = \boldsymbol{\omega} - \boldsymbol{\omega}_{vc} \quad \to \quad \dot{\boldsymbol{z}} = \dot{\boldsymbol{\omega}} - \dot{\boldsymbol{\omega}}_{vc}$$

$$J\dot{\boldsymbol{z}} = \boldsymbol{\tau} - \boldsymbol{\omega} \times (J\boldsymbol{\omega}) - J\boldsymbol{\omega}_{vc}$$

$$\dot{\boldsymbol{q}} = \frac{1}{2}\boldsymbol{q} \otimes (\boldsymbol{z} + \boldsymbol{\omega}_{vc})$$
$$\dot{\boldsymbol{q}} = \frac{1}{2}\boldsymbol{q} \otimes \boldsymbol{z} + \frac{1}{2}\boldsymbol{q} \otimes (-2\boldsymbol{q}^* \otimes \boldsymbol{\nabla V})$$
$$\dot{\boldsymbol{q}} = \frac{1}{2}\boldsymbol{q} \otimes \boldsymbol{z} - \boldsymbol{\nabla V}$$

The new system of $\dot{\boldsymbol{q}}$ and $\dot{\boldsymbol{z}}$ now must be stabilized by some choice of $\boldsymbol{\tau}$. To show this, a *Control Lyapunov Function* (CLF) is chosen under the assumption that the Lyapunov function for the original system dynamics follows $V(\boldsymbol{q}) > 0 \;\; \& \;\; \dot{V}(\boldsymbol{q}) < 0 \;\; \forall \; \boldsymbol{q}$

$$V_z = V + \frac{1}{2}\boldsymbol{z}^\intercal J \boldsymbol{z}$$
$$\dot{V}_z = \dot{V} + \frac{1}{2}\frac{d}{dt}\left(\boldsymbol{z}^\intercal J \boldsymbol{z}\right)$$
$$\dot{V}_z = \dot{V} + \boldsymbol{z}^\intercal J \dot{\boldsymbol{z}} \;\; \text{by } (J = J^\intercal)$$
$$\dot{V}_z = \boldsymbol{\nabla V} \cdot \dot{\boldsymbol{q}} + \boldsymbol{z}^\intercal(\boldsymbol{\tau} - \boldsymbol{\omega} \times (J\boldsymbol{\omega}) - J\dot{\boldsymbol{\omega}}_{vc})$$
$$\dot{V}_z = \boldsymbol{\nabla V} \cdot (\frac{1}{2}\boldsymbol{q} \otimes \boldsymbol{z} - \boldsymbol{\nabla V}) + \boldsymbol{z}^\intercal(\boldsymbol{\tau} - \boldsymbol{\omega} \times (J\boldsymbol{\omega}) - J\dot{\boldsymbol{\omega}}_{vc})$$
$$\dot{V}_z = \boldsymbol{\nabla V}^\intercal(\boldsymbol{q} \otimes \boldsymbol{z}) + \boldsymbol{z}^\intercal(\boldsymbol{\tau} - \boldsymbol{\omega} \times (J\boldsymbol{\omega}) - J\dot{\boldsymbol{\omega}}_{vc}) - \|\boldsymbol{\nabla V}\|^2$$

For the control input $\boldsymbol{\tau}$ to stabilize the system, it must be chosen such that $\dot{V}_z < 0$ for all $\boldsymbol{q}$ and $\boldsymbol{z}$. Further simplification of $\boldsymbol{\nabla V}^\intercal(\boldsymbol{q} \otimes \boldsymbol{z})$ provides a more intuitive choice of $\vec{\tau}$ that ensures $\dot{V}_z < 0$.

$$\boldsymbol{\nabla V}^\intercal(\boldsymbol{q} \otimes \boldsymbol{z}) = \boldsymbol{\nabla V}^\intercal \begin{bmatrix} q_s\vec{z} + \vec{q} \times \vec{z} \\ -\vec{q}^\intercal \vec{z} \end{bmatrix}$$
$$\boldsymbol{\nabla V}^\intercal(\boldsymbol{q} \otimes \boldsymbol{z}) = \begin{bmatrix} \nabla\vec{V}^\intercal & \nabla V_s \end{bmatrix} \begin{bmatrix} q_s\vec{z} + \vec{q} \times \vec{z} \\ -\vec{q}^\intercal \vec{z} \end{bmatrix}$$
$$\boldsymbol{\nabla V}^\intercal(\boldsymbol{q} \otimes \boldsymbol{z}) = \nabla\vec{V}^\intercal q_s\vec{z} + \nabla\vec{V}^\intercal(\vec{q} \times \vec{z}) + \nabla V_s(-\vec{q}^\intercal \vec{z})$$
$$\boldsymbol{\nabla V}^\intercal(\boldsymbol{q} \otimes \boldsymbol{z}) = \vec{z}^\intercal \left(q_s\nabla\vec{V} + \nabla\vec{V} \times \vec{q} - \nabla V_s\vec{q}\right)$$

Substituting this term into back into the Lyapunov function $\dot{V}_z$, the term $\vec{z}^\intercal$ may be factored out. Note that the rest of the Lyapunov function is formulated from pure quaternions so without loss of generality it may be converted to a vector equation with the exception of $\dot{\boldsymbol{\omega}}_{vc}$, whose scalar part would go to zero by $\boldsymbol{z}^\intercal$ anyways.

$$\dot{V}_z = \frac{1}{2}\left(\vec{z}^\intercal\left(q_s\nabla\vec{V} + \nabla\vec{V}\times\vec{q} - \nabla V_s\vec{q}\right)\right) + \boldsymbol{z}^\intercal(\boldsymbol{\tau} - \boldsymbol{\omega}\times(J\boldsymbol{\omega}) - J\dot{\boldsymbol{\omega}}_{vc}) - \|\boldsymbol{\nabla V}\|^2$$
$$\dot{V}_z = \vec{z}^\intercal\left(\frac{1}{2}\left(q_s\nabla\vec{V} + \nabla\vec{V}\times\vec{q} - \nabla V_s\vec{q}\right) + \vec{\tau} - \vec{\omega}\times(J\vec{\omega}) - J\dot{\vec{\omega}}_{vc}\right) - \|\boldsymbol{\nabla V}\|^2$$

Calculating $\dot{\boldsymbol{\omega}}_{vc}$ is necessary to determine a stabilizing control vector $\vec{\tau}$, and while the calculation occurs in the domain of the quaternions the equation describing $\vec{\tau}$ will only require the vector part of the result.

$$\dot{\boldsymbol{\omega}}_{vc} = \frac{d}{dt}\left(-2\boldsymbol{q}^*\otimes\boldsymbol{\nabla V}\right)$$
$$\dot{\boldsymbol{\omega}}_{vc} = -2\left(\boldsymbol{q}^*\otimes\left(\frac{d}{dt}\boldsymbol{\nabla V}\right) + \dot{\boldsymbol{q}}^*\otimes\boldsymbol{\nabla V}\right)$$
$$\dot{\boldsymbol{\omega}}_{vc} = -2\left(\boldsymbol{q}^*\otimes\nabla^2 V\dot{\boldsymbol{q}} + \dot{\boldsymbol{q}}^*\otimes\boldsymbol{\nabla V}\right)$$

Note that the equation of $\dot{\boldsymbol{\omega}}_{vc}$ includes the Hessian of the Lyapunov function, prompting its calculation in the following section. With the current form of $\dot{V}_z = \vec{z}^\intercal(\cdot) - \|\boldsymbol{\nabla V}\|^2$ it becomes evident that the choice of $\vec{\tau}$ should set the parenthetical to be $-\vec{z}$, satisfying the definition of the Lyapunov function. Finally, the resulting stabilizing controller is

$$\boxed{\vec{\tau} = \vec{\omega}\times(J\vec{\omega}) + J\dot{\vec{\omega}}_{vc} - \frac{1}{2}\left(q_s\nabla\vec{V} + \nabla\vec{V}\times\vec{q} - \nabla V_s\vec{q}\right) - \vec{z}} \tag{4.5}$$

Again this result assumes that the Lyapunov function has already been described in advance. In fact, the discussion of the Lyapunov function will follow. The error function is not limited to simply a difference as $\boldsymbol{z} = \boldsymbol{\omega} - \boldsymbol{\omega}_{vc}$. The error variable can be defined as $\boldsymbol{z} = \alpha\tan^{-1}(\beta(\boldsymbol{\omega} - \boldsymbol{\omega}_{vc}))$ in [23] or $\boldsymbol{z} = \beta(\boldsymbol{\omega} - \boldsymbol{\omega}_{vc}) - \frac{(\beta(\boldsymbol{\omega}-\boldsymbol{\omega}_{vc}))^3}{3}$ in [38], which yields $\boldsymbol{z} = \beta(\boldsymbol{\omega} - \boldsymbol{\omega}_{vc}) - \frac{\beta^3}{3}((\boldsymbol{\omega} - \boldsymbol{\omega}_{vc})^\intercal(\boldsymbol{\omega} - \boldsymbol{\omega}_{vc}))^3(\vec{n}\sin\left(\frac{3\theta}{2}\right))$ for ordinary quaternions. The first construction is used in the simulation to minimize the initial control efforts.

4.3.1 Control Lyapunov Function with Logarithmic Barrier Functions

The method presented in this section allows the controller to avoid particular attitudes in space, and is a version of a controller defined in [23] applied solely to the ordinary quaternion part of the feedback. The controller is determined by back-stepping using a logarithmic control barrier function. For completeness, the derivation of the terms in the paper are shown here in their entirety. With some boresight vector $\vec{y}^{\mathcal{B}}$ and some sensitive inertial direction vector as $\vec{x}^{\mathcal{I}}$ the constraint is such that $(\vec{x}^{\mathcal{I}})^{\intercal}\vec{y}^{\mathcal{I}} \leqslant \cos(\theta_C)$. Note that the angle between the boresight and sensitivity vector is simply defined as θ. The value θ_C indicates a half angle cone surrounding the sensitivity vector. This inequality can be expressed in quadratic form by the following.

$$M(\theta_C) = \begin{bmatrix} A(\theta_C) & \vec{b} \\ \vec{b}^T & d(\theta_C) \end{bmatrix} \tag{4.6}$$

Where the entries in $M(\theta_C)$ are defined by $d(\theta_C) = (\vec{x}^{\mathcal{I}})^{\intercal}\vec{y}^{\mathcal{B}} - \cos(\theta_C)$, by $A(\theta_C) = \vec{x}^{\mathcal{I}}(\vec{y}^{\mathcal{B}})^{\intercal} + \vec{y}^{\mathcal{B}}\vec{x}^{\intercal} - \left((\vec{x}^{\mathcal{I}})^{\intercal}\vec{y}^{\mathcal{B}} + \cos(\theta_C)\right)\boldsymbol{I}_3$, and by $\vec{b} = \vec{x}^{\mathcal{I}} \times \vec{y}^{\mathcal{B}}$. Equation 4.6, when left and right multiplied by $\boldsymbol{q}_{B/I}$ will convert the vector $\vec{y}^{\mathcal{B}}$ used to form the matrix to $\vec{y}^{\mathcal{I}}$ internally. This is shown in detail in Appendix A. For a forbidden zone, the Lyapunov function is assumed to take the form

$$V_q(\boldsymbol{q}) = \|\boldsymbol{q}_r^* \otimes \boldsymbol{q} - \mathbf{1}\|^2 \left(-k \ln\left(\frac{-\boldsymbol{q}^{\intercal} M(\theta_C)\boldsymbol{q}}{2}\right)\right) \tag{4.7}$$

It's evident that the error quaternion $\boldsymbol{q}_r \otimes \boldsymbol{q} = \mathbf{1}$ is the point at which V_q is zero. The matrix $M(\theta_C)$ is a positive definite matrix whose maximum and minimum eigenvalues are bounded. Details about the matrix $M(\theta_C)$ can be found in Appendix B. Showing that this

Lyapunov function is negative definite, the following relationships are shown for clarity.

$$\begin{aligned}
\|\boldsymbol{q}_r^* \otimes \boldsymbol{q} - \mathbf{1}\|^2 &= 2 - 2\boldsymbol{q}_r^\intercal \boldsymbol{q} \\
\frac{d}{d\boldsymbol{q}} \left\{2 - 2\boldsymbol{q}_r^\intercal \boldsymbol{q}\right\} &= -2\boldsymbol{q}_r^\intercal \\
\frac{d}{d\vec{x}}(\vec{a}^\intercal \vec{x}) &= \vec{a} \\
\frac{d}{d\vec{x}}(\vec{x}^\intercal A \vec{x}) &= (A + A^\intercal)\vec{x} = 2\vec{x}^\intercal A \quad (\text{if } A^\intercal = A)
\end{aligned}$$

Taking the gradient of Equation 4.7 with respect to $\boldsymbol{q}$:

$$\nabla V_q = -k \left(\frac{d\left\{\|\boldsymbol{q}_r^* \otimes \boldsymbol{q} - \mathbf{1}\|^2\right\}}{d\boldsymbol{q}} \ln\left(\frac{-\boldsymbol{q}^\intercal M(\theta_C)\boldsymbol{q}}{2}\right) + \|\boldsymbol{q}_r^* \otimes \boldsymbol{q} - \mathbf{1}\|^2 \frac{d\left\{\ln\left(\frac{-\boldsymbol{q}^\intercal M(\theta_C)\boldsymbol{q}}{2}\right)\right\}}{d\boldsymbol{q}} \right)$$

The resulting gradient is then found to be

$$\boxed{\nabla V_q = 2\boldsymbol{q}_r^\intercal \left(k \ln\left(\frac{\boldsymbol{q}^\intercal M(\theta_C)\boldsymbol{q}}{2}\right)\right) + \|\boldsymbol{q}_r^* \otimes \boldsymbol{q} - \mathbf{1}\|^2 \frac{-2k}{\boldsymbol{q}^\intercal M(\theta_C)\boldsymbol{q}} \boldsymbol{q}^\intercal M(\theta_C)} \tag{4.8}$$

This is the gradient that will be used as mentioned in Section 4.3 for Equation 4.5. This takes into account a single forbidden attitude. For multiple, such as in the simulation, this process is simply repeated and summed. The Hessian is still necessary fo the controller, which must also be positive definite. This is shown in Appendix B. To ease the derivation Equation 4.8 is separated into two terms.

$$T_1 = 2\boldsymbol{q}_r^\intercal \left(k \ln\left(\frac{-\boldsymbol{q}^\intercal M(\theta_C)\boldsymbol{q}}{2}\right)\right) \qquad \text{and} \qquad T_2 = \|\boldsymbol{q}_r^* \otimes \boldsymbol{q} - \mathbf{1}\|^2 \frac{-2k}{\boldsymbol{q}^\intercal M(\theta_C)\boldsymbol{q}} \boldsymbol{q}^\intercal M(\theta_C)$$

Starting with term T_1

$$\begin{aligned}
\nabla T_1 &= 2\boldsymbol{q}_r \frac{d}{d\boldsymbol{q}} \left\{k \ln\left(\frac{-\boldsymbol{q}^\intercal M(\theta_C)\boldsymbol{q}}{2}\right)\right\} + \frac{d}{d\boldsymbol{q}} \left\{2\boldsymbol{q}_r\right\} \ln\left(\frac{-\boldsymbol{q}^\intercal M(\theta_C)\boldsymbol{q}}{2}\right) \\
\nabla T_1 &= \frac{4k\boldsymbol{q}_r \boldsymbol{q}^\intercal M(\theta_C)}{\boldsymbol{q}^\intercal M(\theta_C)\boldsymbol{q}} + 0_{4\times 4}
\end{aligned}$$

Continuing on to term ∇T_2

$$\nabla T_2 = \frac{d}{d\boldsymbol{q}} \left\{\|\boldsymbol{q}_r^* \otimes \boldsymbol{q} - \mathbf{1}\|^2\right\} \frac{-2k\boldsymbol{q}^\intercal M(\theta_C)}{\boldsymbol{q}^\intercal M(\theta_C)\boldsymbol{q}} + \|\boldsymbol{q}_r^* \otimes \boldsymbol{q} - \mathbf{1}\|^2 \frac{d}{d\boldsymbol{q}} \left\{\frac{-2k}{\boldsymbol{q}^\intercal M(\theta_C)\boldsymbol{q}} \boldsymbol{q}^\intercal M(\theta_C)\right\}$$

$$\frac{d}{d\boldsymbol{q}}\left\{\frac{-2k}{\boldsymbol{q}^\intercal M(\theta_C)\boldsymbol{q}}M(\theta_C)\boldsymbol{q}\right\} = \frac{d}{d\boldsymbol{q}}\left\{\frac{-2k}{\boldsymbol{q}^\intercal M(\theta_C)\boldsymbol{q}}\right\}\boldsymbol{q}^\intercal M(\theta_C) + \frac{-2k}{\boldsymbol{q}^\intercal M(\theta_C)\boldsymbol{q}}\frac{d}{d\boldsymbol{q}}\left\{M(\theta_C)\boldsymbol{q}\right\}$$
$$\frac{d}{d\boldsymbol{q}}\left\{\frac{-2k}{\boldsymbol{q}^\intercal M(\theta_C)\boldsymbol{q}}M(\theta_C)\boldsymbol{q}\right\} = \frac{d}{d\boldsymbol{q}}\left\{\frac{-2k}{\boldsymbol{q}^\intercal M(\theta_C)\boldsymbol{q}}\right\}\boldsymbol{q}^\intercal M(\theta_C) + \frac{-2k}{\boldsymbol{q}^\intercal M(\theta_C)\boldsymbol{q}}M(\theta_C)$$
$$\frac{d}{d\boldsymbol{q}}\left\{\frac{-2k}{\boldsymbol{q}^\intercal M(\theta_C)\boldsymbol{q}}M(\theta_C)\boldsymbol{q}\right\} = \frac{4k\left(\boldsymbol{q}^\intercal M\right)^\intercal}{\left(\boldsymbol{q}^\intercal M(\theta_C)\boldsymbol{q}\right)^2}\boldsymbol{q}^\intercal M(\theta_C) + \frac{-2k}{\boldsymbol{q}^\intercal M(\theta_C)\boldsymbol{q}}M(\theta_C)$$
$$\frac{d}{d\boldsymbol{q}}\left\{\frac{-2k}{\boldsymbol{q}^\intercal M(\theta_C)\boldsymbol{q}}M(\theta_C)\boldsymbol{q}\right\} = \frac{4k(\boldsymbol{q}^\intercal M(\theta_C))^\intercal\boldsymbol{q}^\intercal M(\theta_C)}{\left(\boldsymbol{q}^\intercal M(\theta_C)\boldsymbol{q}\right)^2} + \frac{-2kM(\theta_C)}{\boldsymbol{q}^\intercal M(\theta_C)\boldsymbol{q}}$$

Combining all the terms in ∇T_2:

$$\nabla T_2 = \frac{4k\boldsymbol{q}_r}{\boldsymbol{q}^\intercal M(\theta_C)\boldsymbol{q}}\boldsymbol{q}^\intercal M(\theta_C) + \|\boldsymbol{q}_r^* \otimes \boldsymbol{q} - \mathbf{1}\|^2\left(\frac{4k(\boldsymbol{q}^\intercal M(\theta_C))^\intercal\boldsymbol{q}^\intercal M(\theta_C)}{\left(\boldsymbol{q}^\intercal M(\theta_C)\boldsymbol{q}\right)^2} + \frac{-2kM(\theta_C)}{\boldsymbol{q}^\intercal M(\theta_C)\boldsymbol{q}}\right)$$

Then jointly, the Hessian of the Lyapunov function $\nabla^2 V$ is the sum $\nabla T_1 + \nabla T_2$.

4.4 Synthesis of Controller

For the completion of the formulation of the control law, a method is presented here to combine the attitude constraint avoidance from Equation 4.5 and Equation 4.4 to rendezvous with another spacecraft under pointing constraints. First rewriting the PD controller more conveniently:

$$\tilde{\boldsymbol{f}}^{\mathcal{B}} = -k_p(\tilde{\mathbf{q}}^*_{B/G} \circledast (\tilde{\mathbf{q}}^s_{B/G} - \tilde{\mathbf{1}}^s)) - 2(\tilde{\mathbf{q}}^*_{B/G} \circledast \tilde{\boldsymbol{z}}^s_f)$$
$$\tilde{\boldsymbol{f}}^{\mathcal{B}} = \begin{bmatrix} -k_p\boldsymbol{q}^*_{B/G}\boldsymbol{d}_{B/G} - 2\boldsymbol{q}^*_{B/G}\boldsymbol{z}_{fd} + \text{R.T.} \\ -k_p\boldsymbol{d}^*_{B/G} \otimes (\boldsymbol{q}_{B/G} - \mathbf{1}) - 2(\boldsymbol{d}^*_{B/G} \otimes \boldsymbol{z}_{fd} + \boldsymbol{q}_{B/G} \otimes \boldsymbol{z}_f) + \text{R.T.} \end{bmatrix}$$

Where R.T. represents the relative terms. Since the controller calls for the vector part, and all of the relative terms will also be pure, the above can be considered a pure quaternion. Revisiting the back-stepping controller and rewriting it as a quaternion equation,

$$\vec{\tau} = \vec{\omega} \times (J\vec{\omega}) + J\dot{\vec{\omega}}_{vc} - \frac{1}{2}\left(q_s \nabla\vec{V} + \nabla\vec{V} \times \vec{q} - \nabla V_s \vec{q}\right) - \vec{z}_e$$

$$\boldsymbol{\tau} = \begin{bmatrix} \vec{\omega} \times (J\vec{\omega}) + J\dot{\vec{\omega}}_{vc} - \frac{1}{2}\left(q_s \nabla\vec{V} + \nabla\vec{V} \times \vec{q} - \nabla V_s \vec{q}\right) - \vec{z}_e \\ 0 \end{bmatrix}$$

Then the two can be jointly summed to form the combined controller as follows:

$$\boxed{\tilde{\boldsymbol{f}}^{\mathcal{B}} = \begin{bmatrix} \boldsymbol{\tau} - k_p \boldsymbol{q}^*_{B/G} \boldsymbol{d}_{B/G} - 2\boldsymbol{q}^*_{B/G} \boldsymbol{z}_{fd} \\ -k_p \boldsymbol{d}^*_{B/G} \otimes (\boldsymbol{q}_{B/G} - \mathbf{1}) - 2(\boldsymbol{d}^*_{B/G} \otimes \boldsymbol{z}_{fd} + \boldsymbol{q}_{B/G} \otimes \boldsymbol{z}_{fp}) \end{bmatrix}} \tag{4.9}$$

Where the values $\boldsymbol{\nabla V}$, $\boldsymbol{z}_f$, and $\boldsymbol{\tau}$ are calculated based off of the formulations in Sections 4.1, 4.3, and 4.3.1. The value $\vec{z}_e$ in $\boldsymbol{\tau}$ is determined by the system

$$\dot{\tilde{\boldsymbol{x}}}_f = A\tilde{\boldsymbol{x}}_f + B\tilde{\mathbf{q}}_{B/G} \tag{4.10}$$

$$\tilde{\boldsymbol{z}} = CA\tilde{\boldsymbol{x}}_f + CB\tilde{\mathbf{q}}_{B/G} \tag{4.11}$$

The combination of these two controllers is the primary contribution of the work, alongside the formulation of the area frame and aerodynamic model in Section 3.2. Each of the controllers individually have resources describing some of the qualities of each controller such as in [23, 13, 39]. The combination of these controllers and the subsequent analysis is

Chapter 5

RESULTS AND ANALYSIS

The dynamic system described in Chapter 3 is simulated in MATLAB to present the performance of the controller designed in Chapter 4. For the simulation, the classical orbital elements describing the test orbits are listed in Table 3.1 are used. Each of these orbital cases is compared against a baseline case with values specified in Table 3.2. Rendezvous in this context is considered to be when the spacecraft approaches to within one to two meters of the desired frame having avoided unwanted attitudes within a reasonable span of time.

Case	$\vec{r}^{\mathcal{I}}_{G/I}$	$\vec{v}^{\mathcal{I}}_{G/I}$
LEO	[6771.2, 0, 0] km	[0, 7.6725, 0] $\frac{\text{km}}{\text{s}}$
Maratus	[-2398, 5762, 3068.3] km	[-6.6594, -3.4055, 1.2234] $\frac{\text{km}}{\text{s}}$
Inertial Constraint	$\vec{y}^{\mathcal{I}}$	θ_C
1	[1, 0, 0]	15°
2	[-1, 0, 0]	15°
3	$\left[0, -\frac{\sqrt{2}}{2}, \frac{\sqrt{2}}{2}\right]$	30°

Table 5.1: Orbital conditions and attitude constraints

Each case will be simulated under the effect of the orbital disturbances listed in Section 3.2 without the filtered measurement from Equation 4.2 unless otherwise specified. For the sake of consistency, the initial position and velocity used for each of the cases are listed in Table 5.1.

5.1 LEO Case

The LEO case presents a satellite in a circular equatorial orbit with a 400 km altitude. A progressive approach is taken to demonstrate the performance of the combined controller by showing the results of the controller described in Section 4.1, the PD case are shown first. Then, the attitude constraints based off of the back-stepping controller from Section 4.3 and Section 4.3.1 (CBF case) is second. Finally, the combined controller is analyzed, as a means to compare the benefit of joining the two together.

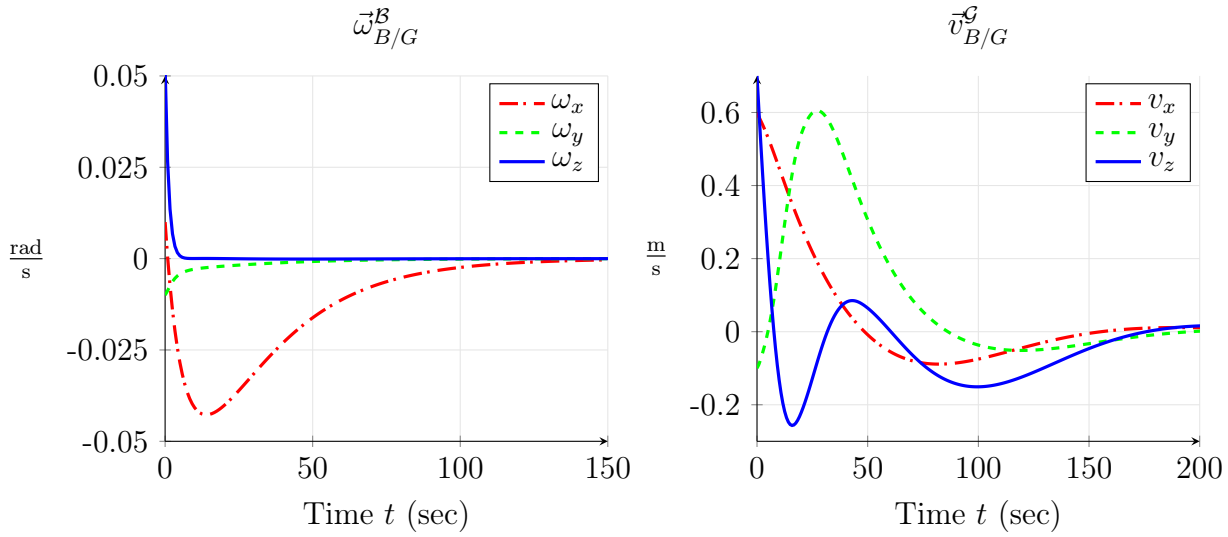

(a) Angular velocity in $\mathcal{B}$: PD

(b) Relative linear velocity in $\mathcal{G}$: PD

Figure 5.1: LEO case with PD: Velocities over time

The PD controller shown in Figure 5.1 presents a fast response time for the angular velocity, which is expected as there are no attitude constraints imposed. The linear velocity does take notably longer to reach an equilibrium. However, this is reasonable given that the means to reorient in low Earth orbit is typically more accessible. High relative velocities inherently pose a risk of impact where imposing slower approach speeds is both effectively required in rendezvous maneuvers.

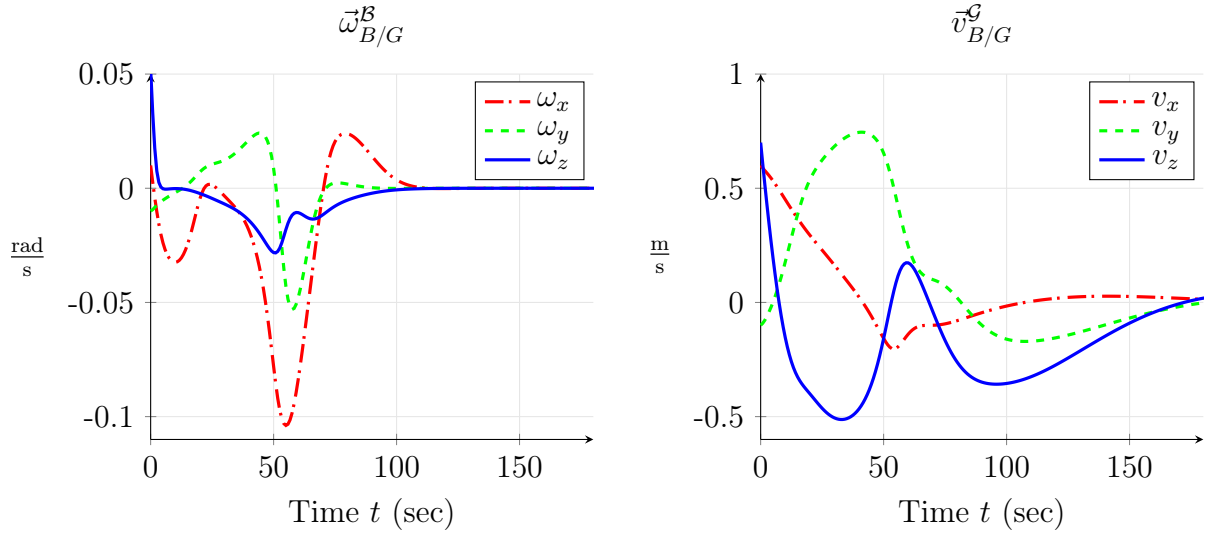

(a) Angular velocity in $\mathcal{B}$: CBF

(b) Relative linear velocity in $\mathcal{B}$: CBF

Figure 5.2: LEO case with CBF: Velocities over time

In comparison with the PD controller alone in Figure 5.1, the control barrier function appears to perform much differently. Of course, the duration of time for the pose to reach the desired location in space is increased as the controller must take time to avoid the constraints imposed onto the system. The angular velocity does change rapidly in Figure 5.2a, which can be corrected by choice of k_{CBF}. In some cases with this control scheme, the spacecraft may take a longer route to arrive at the commanded orientation, a result of the *unwinding* phenomena.

The choice of controller for the CBF case was initially intended for reorientation under attitude constraints [23], so the impact of the controller is only applied to the dual part of the system. This does not render the linear component trivially ignored however. The velocity in Figure 5.2b shows the effect of sudden rotations provoking a rapid change in the relative linear velocity in the $\mathcal{B}$ frame. Measurements are typically taken from the perspective of a spacecraft - or in the frame of the sensors on board. This change inside of frame $\mathcal{B}$ could

pose a notable challenge in terms of measurement and estimation.

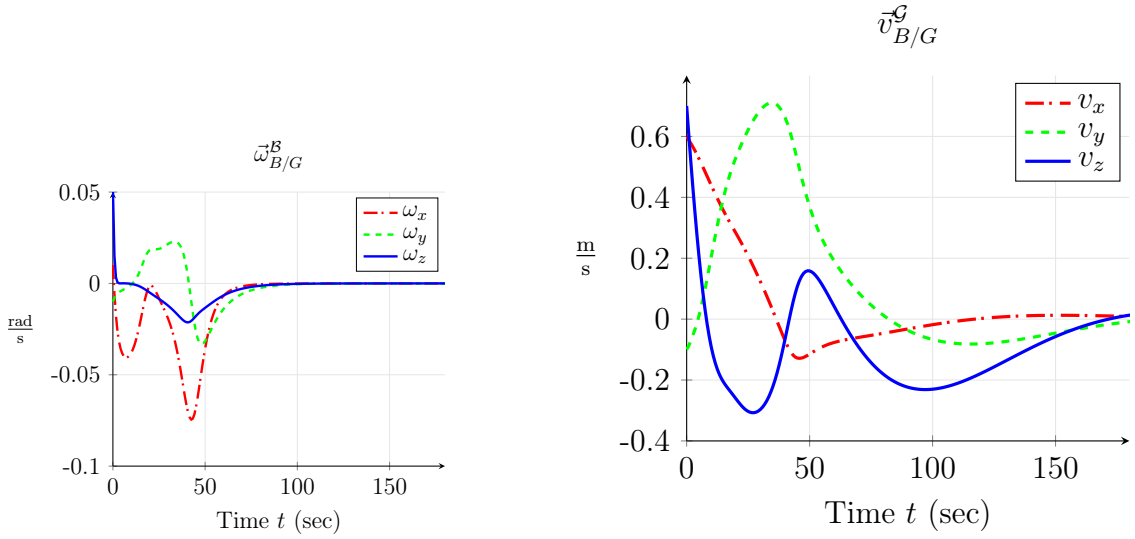

(a) Angular velocity in $\mathcal{B}$: Combined

(b) Relative linear velocity in $\mathcal{B}$: Combined

Figure 5.3: LEO case with combined controller: Velocities over time

Once combined, the PD controller and the CBF controller work together to reorient and reposition the spacecraft to align with the axes of $\mathcal{G}$. The effects of this combination is particularly visible in Figure 5.3a, where the relative angular velocity is quickly decreased while avoiding the unwanted orientation zones and the effects of the unwinding phenomenon. The relative linear velocity shows similarly long settling times for the position when compared with Figure 5.2, but with much smaller magnitudes in each given direction, a desirable trait for preventing accidents.

It should be reiterated that sudden changes in the velocity measurements shown in both Figure 5.2 and 5.3 may correspond with increased uncertainty in the system during a rapid slewing. During the later stages of rendezvous the relative velocities are often small, but with noise and other system uncertainties it may pose an unwanted danger upon failure of some subsystems, sensors, or actuators. Further discussion is left in Section 5.3.

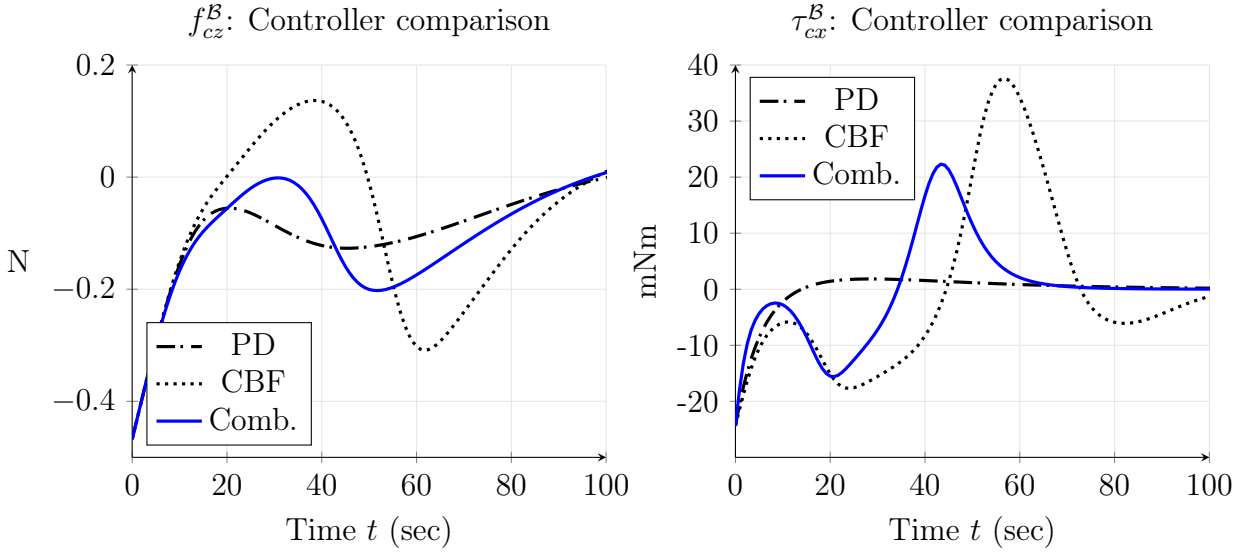

(a) Control forces in $\mathcal{B}_z$

(b) Control torques in $\mathcal{B}_x$

Figure 5.4: Comparison of control efforts in selected axes

For the sake of brevity only the control forces in the $\mathcal{B}_z$ axis and the control torques in the $\mathcal{B}_x$ axis are shown here in Figure 5.4a. For a complete picture Figures C.1 and C.2 present the other respective axes. The results for the PD controller generally align with what is to be expected from a classical standpoint and uses the least amount of energy in the baseline case - but it does not account for attitude constraints. For the control torques on the system, a similar conclusion can be made, but with the caveat that the CBF controller does have 'smoother' paths when re-orienting around attitude constraints. Of course, this is also an idealized situation where orbital perturbations will generally be smaller in comparison to the Maratus case, where the comparison of the controllers by variation in the control gains is discussed.

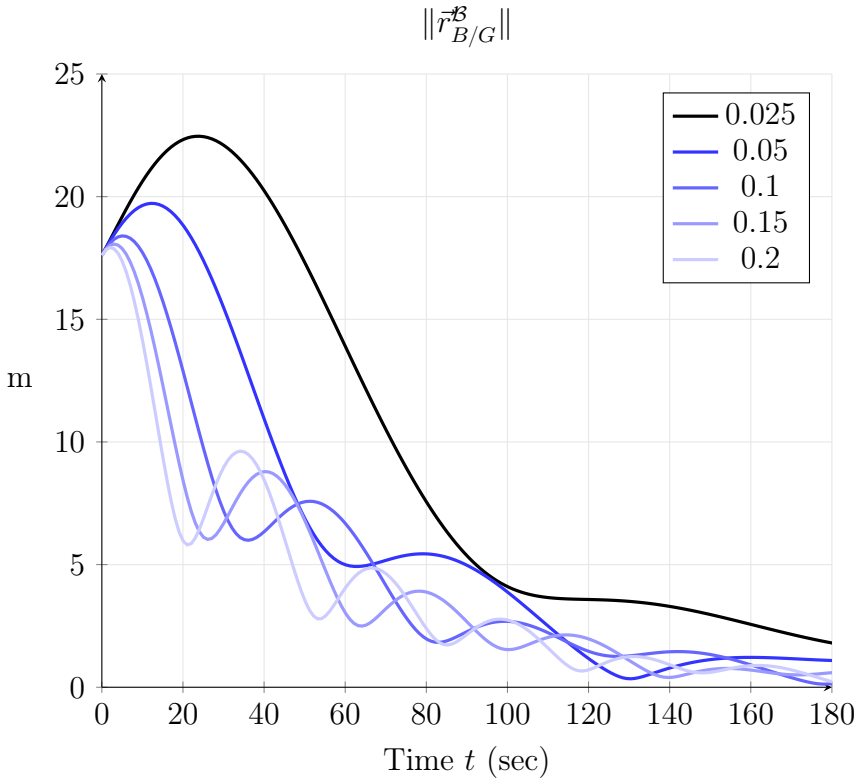

Figure 5.5: k_p vs. $\|\vec{r}^{\mathcal{B}}_{B/G}\|$: PD Controller

5.2 Maratus Case

The Maratus case is chosen as a more realistic situation for the inclusion of orbital disturbances in comparison with the circular orbit given in the LEO case. For better clarity in the response of the system the filter is not used, and a direct measurement for the relative motor is assumed for the Maratus case to better express the change with varying parameters. Most of the parameters listed in Table 3.2 are varied over the duration of the rendezvous within reasonably selected bounds to prevent excessive responses or unrealistic behavior. The goal is to express the change in the system with respect to the given variables by choosing a metric that shows the change most directly. When possible and reasonable the corresponding plots for other controllers, cases, and metrics are included in Appendix C.

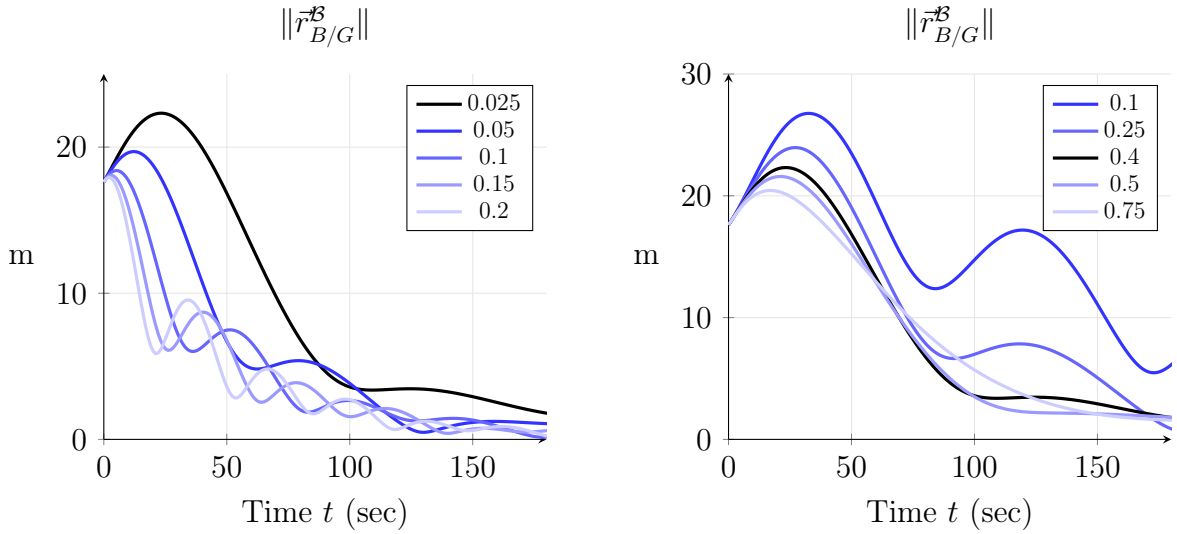

(a) k_p vs. $\|\vec{r}^{\mathcal{B}}_{B/G}\|$

(b) k_d vs. $\|\vec{r}^{\mathcal{B}}_{B/G}\|$

Figure 5.6: $\|\vec{r}^{\mathcal{B}}_{B/G}\|$ vs. k_p and k_d for combined controller

First, the variance of the PD gains is shown on the combined controller with respect to its position. The magnitude of $\|\vec{r}^{\mathcal{B}}_{B/G}\|$ is used to show the absolute distance between the two frames. As for the baseline condition, shown in black, the initial distance increases solely by nature of the initial velocity relative to the $\mathcal{G}$ frame, and shortly begins its approach. As the proportional constant increases, the relative position oscillates around $\mathcal{G}$, causing the oscillations shown in Figures 5.6a and 5.6b. With the initial velocity being small and the two frames being proximate, Here a slow approach is desirable to lower the chance of impact. The lower gain k_p may also prevent the system from responding quickly enough if the situation requires a faster response. With larger initial relative velocities the initial peak will increase as the control is much smaller, potentially causing unwanted relative orbiting.

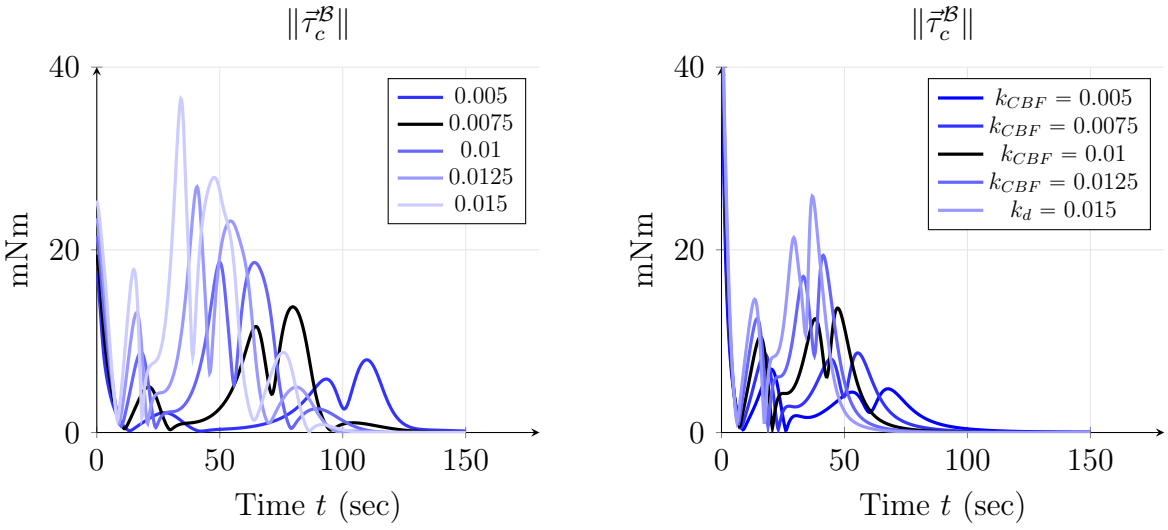

(a) CBF

(b) Combined controller

Figure 5.7: $\|\vec{\tau}_c^{\mathcal{B}}\|$ vs. k_{CBF} for combined controller and CBF

For the variance with relation to the gain k_{CBF}, note that the initial command for the control torque is actually higher in the combined controller when compared to the the CBF case, and for smaller satellites would potentially reach control saturation. This comes with a reduced overall settling time and energy usage after the initial commanded values. The gain k_{CBF} is also much more sensitive to change when compared to other gains, so the selection of this value must be made carefully to ensure that the control efforts do not surpass physical limits of the satellite or cause unrealistic results.

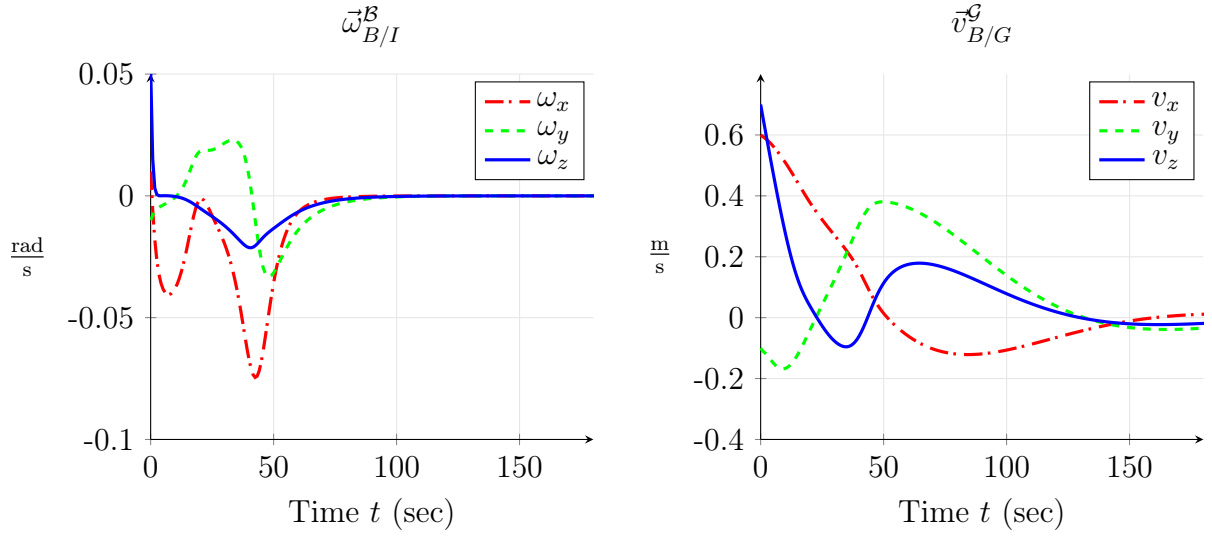

(a) Angular velocity in $\mathcal{B}$

(b) Relative linear velocity in $\mathcal{B}$

Figure 5.8: Maratus Case with combined controller: Velocities over time

To complete the comparison to the LEO case, the angular and linear velocities expressed in the $\mathcal{B}$ frame are shown for the combined controller in Figure 5.8. The linear velocity in the body decays at about the same rate, whereas the angular velocity decays much faster than what is shown in Figure C.4. This makes some intuitive sense as the combination of the PD and CBF components is in the ordinary part of the control wrench, affecting the orientation strongly, and carrying through to the linear components by extension. As a final comparison between the controllers, the CBF and combined controller pure quaternion components are plotted against one another in Figure. 5.9

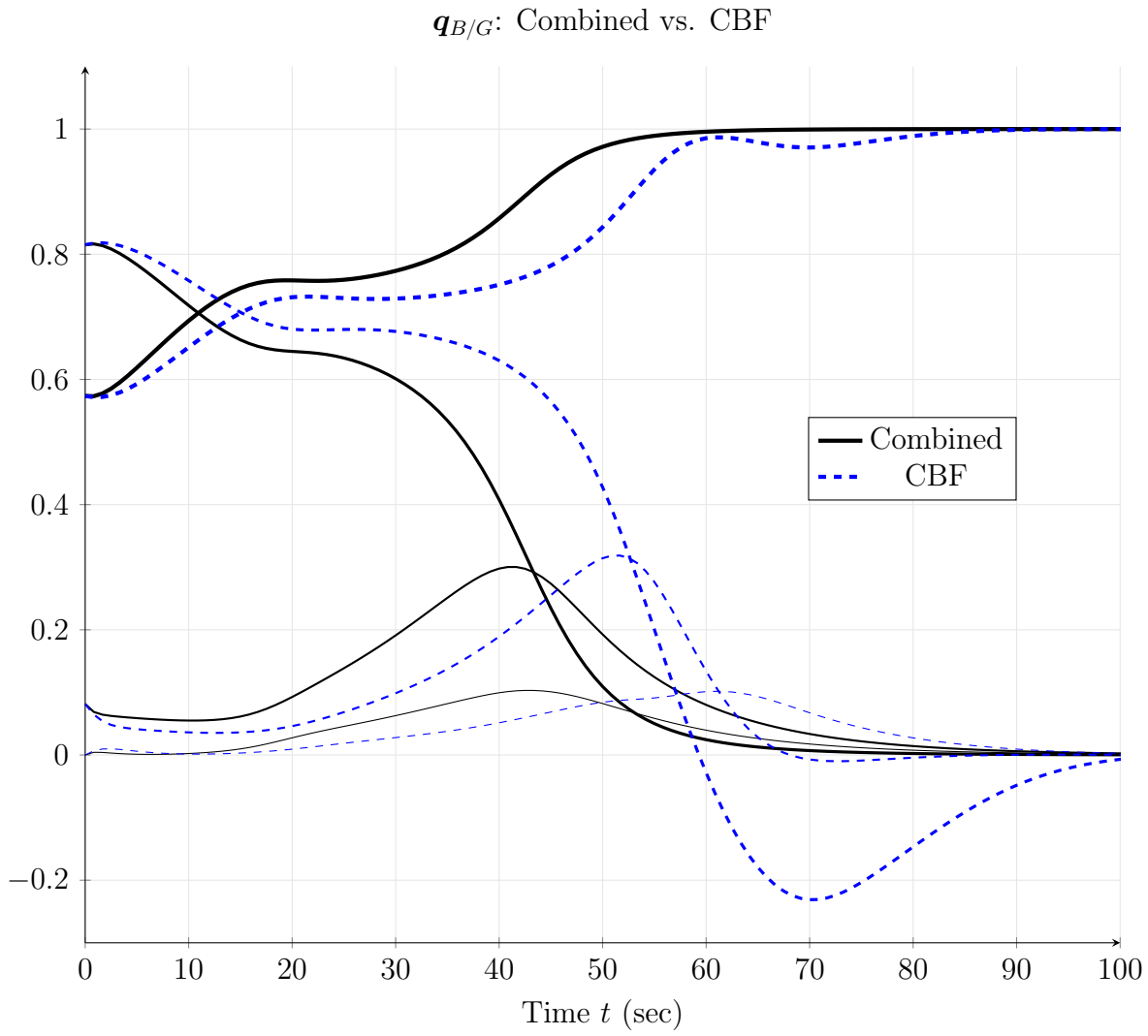

Figure 5.9: $\boldsymbol{q}_{B/G}$ for Combined Controller and CBF

5.3 Limitations of Methodology and Future Work

One of the most notable limitations is the lack of bounds on the control effort, particularly for the commanded thrust. Thrust is simulated as if it is generated continuously and without a limit. Care has been taken to consider this in the controller design to generate realistic bounds in the baseline case but having some limitation on the control wrench would be an improvement. With limits in place then control allocation for reaction wheels, magnetorquers and thrusters would then be be a welcome addition.

Beyond the physical component the discretization of the controller is another valuable next step for future work, as discrete time analysis is not included in this work. The combination of discretization with control allocation would provide a good testbed controller for dual quaternions for various labs with 5DOF testing abilities. Additionally, some constraint on the dual quaternion as a whole is mentioned in [24] for planetary landing problems which presents the constraint as an angle with respect to some landing site, analogous to the attitude constraints described in Chapter 4 for some boresight. An extension of this could be imposing some form of unit ball constraint on the position. This would exacerbate the aforementioned issue of control effort limitations but would be an interesting endeavor.

While the PD controller is shown to be stable in the sense of Lyapunov over time in [13, 14, 39] and the same is provided in the Appendices and in [23, 24], the assumption is that the inertial vectors do not move over time. In [13] the transient component of the Lyapunov is discussed, but for the logarithmic barrier functions the inertial vectors are assumed to be stationary in $\mathcal{I}$, whereas a time varying inertial constraint could have useful application. Robustness is not deeply taken into consideration in this work and trivial cancellations are made within the derivation of the back-stepping controller. In particular, uncertainty in the dual inertia matrix would be a good place to further develop the controller. The controller as presented in 4.9 does not have 'memory' and uses the low-pass dual quaternion filter to account for the lack of velocity measurements. In a higher accuracy simulation a Kalman filter would be a good addition to the system, discrete or otherwise.

BIBLIOGRAPHY

[1] Edwin (Buzz) Aldrin. *Line-of-sight guidance techniques for manned orbital rendezvous*. PhD thesis, Massachusetts Institute of Technology, 1963.

[2] Thawar T. Arif. Adaptive control of rigid body satellite. *International Journal of Automation and Computing*, 5(3):296–306, Jul 2008.

[3] Jon Arrizabalaga and Markus Ryll. Pose-following with dual quaternions. In *2023 62nd IEEE Conference on Decision and Control (CDC)*, pages 5959–5966, 2023.

[4] J B Barlow, W H Rae, and A Pope. *Low Speed Wind Tunnel Testing*. John Wiley and Sons, Hoboken, 1999.

[5] V. Brodsky and M. Shoham. Dual numbers representation of rigid body dynamics. *Mechanism and machine theory*, 34(5):693–718, 1999.

[6] Terrance Carney. An automatic terminal guidance system for rendezvous with a satellite. *NASA Technical Note*, D-923, August 1961.

[7] McDonell Douglas Technical Services Co. Euler angles, quaternions, and transformation matrices for space shuttle analysis. *NASA*, Jun 1977.

[8] Michael J. Crowe. A history of vector analysis : the evolution of the idea of a vectorial system, 1967.

[9] Howard D. Curtis. *Orbital Mechanics for Engineering Students*. Katey Birtcher, 2020.

[10] Hongyang Dong, Qinglei Hu, and Maruthi R. Akella. Dual-quaternion-based spacecraft autonomous rendezvous and docking under six-degree-of-freedom motion constraints. *Journal of Guidance, Control, and Dynamics*, 41(5):1150–1162, 2018.

[11] John Eggleston. A study of the positions and velocities of a space station and a ferry vehicle during rendezvous and return. *NASA Technical Report*, R-87, August 1961.

[12] João Gutemberg Farias, Edson De Pieri, and Daniel Martins. A review on the applications of dual quaternions. *Machines*, 12(6), 2024.

[13] Nuno Filipe. *Nonlinear Pose Control and Estimation for Space Proximity Operations: An Approach Based on Dual Quaternions*. PhD thesis, Georgia Institute of Technology, 2014.

[14] Nuno Filipe and Panagiotis Tsiotras. Adaptive position and attitude-tracking controller for satellite proximity operations using dual quaternions. *Journal of Guidance, Control, and Dynamics*, 38:566–577, 04 2015.

[15] QJ Ge, Zihan Yu, and Mark Langer. A dual quaternion based method for estimating margins for planning target volumes in radiotherapy, 2020.

[16] DP. Han and ZX. Li. Kinematic control of free rigid bodies using dual quaternions. *Int. J. Autom. Comput.*, 5:319–324, 2008.

[17] Yan-Bin Jia. Dual quaternions. *Iowa State University: Ames, IA, USA*, pages 1–15, 2013.

[18] K P Karthikeyan, H Simha, and H Priyadarshan. A linear discrete time controller for spacecraft attitude dynamics on lie group. In *2016 Indian Control Conference (ICC)*, pages 165–169, 2016.

[19] Ben Kenwright. A Beginners Guide to Dual Quaternions. *George Mason University, Internal*, 2012.

[20] Charles Key (III). *Don't Take My Advice*. Kindle, Washington State, March 2024. See section on 'Accuracy'.

[21] Raymond Kristiansen, Per Johan Nicklasson, and Jan Tommy Gravdahl. Satellite attitude control by quaternion-based backstepping. *IEEE Transactions on Control Systems Technology*, 17(1):227–232, 2009.

[22] John L.Crassidis and F. Landis Markley. *Fundamentals of Spacecraft Attitude Determination and Control*. Springer, 2014.

[23] Unsik Lee and Mehran Mesbahi. Spacecraft reorientation in presence of attitude constraints via logarithmic barrier potentials. In *Proceedings of the 2011 American Control Conference*, pages 450–455, 2011.

[24] Unsik Lee and Mehran Mesbahi. Constrained autonomous precision landing via dual quaternions and model predictive control. *Journal of Guidance, Control, and Dynamics*, 40(2):292–308, 2017.

[25] Alex McAulay. *Octonions : A Development of Clifford's Bi-Quaterions*. Cambridge Press, 1898.

[26] Colm Mulcahy. How a 19th century irish mathematician helped nasa into space. *RTÉ*, October 2019.

[27] ESA Space Debris Office. Esa's annual space environment report. *European Space Agency*, March 2025.

[28] Ian R. Porteous. *Clifford Algebras and the Classical Groups*. Cambridge University Press, 1995.

[29] Taylor P. Reynolds, Michael Szmuk, Danylo Malyuta, Mehran Mesbahi, Behçet Açıkmeşe, and John M. Carson. *Dual Quaternion-Based Powered Descent Guidance with State-Triggered Constraints*. Journal of Guidance, Control, and Dynamics, 2020.

[30] Anton H.J. De Ruiter, Christopher J. Damaren, and James R. Forbes. *Spacecraft Dynamics & Control: An Introduction*. John Wiley & Sons Ltd., 2013.

[31] Alfredo Valverde Salazar. *Dynamic Modeling and Control of Spacecraft Robotic Systems Using Dual Quaternions*. PhD thesis, Georgia Institute of Technology, 2018.

[32] Marcel J. Sidi. *Spacecraft Dynamics and Control: A Practical Engineering Approach*. Cambridge University Press, 1997.

[33] Kyl Stanfield and Ahmad Bani Younes. Dual-Quaternion Analytic LQR Control Design for Spacecraft Proximity Operations. *Sensors*, 2021.

[34] Brian L. Stevens, Frank L. Lewis, and Eric N. Johnson. *Aircraft Control and Simulation*. John Wiley & Sons Ltd., 2016.

[35] Yuichi Takaku and Yuichi Ikeda. Quaternion-based discrete-time nonlinear attitude tracking control of spacecraft. In *2020 Australian and New Zealand Control Conference (ANZCC)*, pages 75–80, 2020.

[36] Amdreallyfast User. *Quaternions, Dual Numbers, and Dual Quaternions - An Introductory Guide and Computational Comparison with Matrices and Vectors*. Creative Commons., 2015.

[37] Xiangke Wang and Changbin Yu. Unit dual quaternion-based feedback linearization tracking problem for attitude and position dynamics. *Systems & Control Letters*, 62:225–233, 03 2013.

[38] Qiang Zhang and Xianku Zhang. Nonlinear improved concise backstepping control of course keeping for ships. *IEEE Access*, PP:1–1, 01 2019.

[39] Vrushabh Zinage, S. P. Arjun Ram, Maruthi R. Akella, and Efstathios Bakolas. Semiglobal exponential stability for dual-quaternion-based rigid-body tracking control. *Journal of Guidance, Control, and Dynamics*, 47(8):1507–1520, 2024.

Appendix A

DERIVATION/PROOF OF $\boldsymbol{M(\theta_C)}$

This is the derivation for $M(\theta_C)$ showing the transformation of the $\vec{y}^{\mathcal{B}} \rightarrow \vec{y}^{\mathcal{I}}$ by quaternion in the form of $\boldsymbol{q}^\intercal M(\theta_C)\boldsymbol{q}$

$$\vec{y}_I = \vec{y}_B - 2(\vec{q}_v^\intercal \vec{q}_v)y_B + 2(\vec{q}_v^\intercal \vec{y}_B)\vec{q}_v + 2q_s(\vec{y}_B \times \vec{q}_v)$$

$$\begin{aligned}
M(\theta_C) &= \begin{bmatrix} A(\theta) & b \\ b^T & d(\theta) \end{bmatrix} \\
A(\theta) &= \vec{x}\vec{y}^\intercal + \vec{y}\vec{x}^\intercal - (\vec{x}^\intercal \vec{y} + \cos(\theta))\,\boldsymbol{I}_3 \\
d(\theta) &= \vec{x}^\intercal \vec{y} - \cos(\theta) \\
b &= \vec{x} \times \vec{y} \\
\boldsymbol{q}^\intercal M(\theta_C)\boldsymbol{q} &= \boldsymbol{q}^\intercal \begin{bmatrix} A(\theta) & b \\ b^T & d(\theta) \end{bmatrix} \boldsymbol{q} \\
&= \begin{bmatrix} \vec{q}_v^\intercal & q_s \end{bmatrix} \begin{bmatrix} A(\theta) & b \\ b^T & d(\theta) \end{bmatrix} \begin{bmatrix} \vec{q}_v \\ q_s \end{bmatrix} \\
&= \begin{bmatrix} \vec{q}_v^\intercal & q_s \end{bmatrix} \begin{bmatrix} A(\theta)\vec{q}_v + bq_s \\ b^\intercal \vec{q}_v + d(\theta)q_s \end{bmatrix} \\
&= \vec{q}_v^\intercal \left(A(\theta)\vec{q}_v + bq_s\right) + q_s(b^\intercal \vec{q}_v + d(\theta)q_s) \\
&= \vec{q}_v^\intercal A(\theta)\vec{q}_v + bq_s\vec{q}_v^\intercal + q_s b^\intercal \vec{q}_v + q_s^2 d(\theta)
\end{aligned}$$

$$
\begin{aligned}
\boldsymbol{q}^\intercal M(\theta_C)\boldsymbol{q} &= \vec{q}_v^\intercal(\vec{x}\vec{y}^\intercal + \vec{y}\vec{x}^\intercal - (\vec{x}^\intercal\vec{y} + \cos(\theta))\boldsymbol{I}_{3\times 3})\vec{q}_v + \vec{q}_v^\intercal(\vec{x}\times\vec{y})q_s + q_s(\vec{x}\times\vec{y})^\intercal\vec{q}_v + q_s^2(\vec{x}^\intercal\vec{y} - \cos(\theta))) \\
&= \vec{q}_v^\intercal(\vec{x}\vec{y}^\intercal + \vec{y}\vec{x}^\intercal)\vec{q}_v - (\vec{x}^\intercal\vec{y} - \cos(\theta))\vec{q}_v^\intercal\vec{q}_v + 2q_s\vec{q}_v^\intercal(\vec{x}\times\vec{y}) + q_s^2(\vec{x}^\intercal\vec{y} - \cos(\theta)) \\
&= (\vec{q}_v^\intercal\vec{x})(\vec{y}^\intercal\vec{q}_v) + (\vec{q}_v^\intercal\vec{y})(\vec{x}^\intercal\vec{q}_v) - (\vec{x}^\intercal\vec{y})\vec{q}_v^\intercal\vec{q}_v - \cos(\theta)\vec{q}_v^\intercal\vec{q}_v + 2q_s\vec{q}_v^\intercal(\vec{x}\times\vec{y}) + q_s^2(\vec{x}^\intercal\vec{y} - \cos(\theta)) \\
&= 2(\vec{q}_v^\intercal\vec{y})(\vec{q}_v^\intercal\vec{x}) - (\vec{x}^\intercal\vec{y})\vec{q}_v^\intercal\vec{q}_v + 2q_s\vec{q}_v^\intercal(\vec{x}\times\vec{y}) + q_s^2\vec{x}^\intercal\vec{y} + (-\vec{q}_v^\intercal\vec{q}_v - q_s^2)\cos(\theta) \leqslant 0 \\
&= 2(\vec{q}_v^\intercal\vec{y})(\vec{q}_v^\intercal\vec{x}) - (\vec{x}^\intercal\vec{y})\vec{q}_v^\intercal\vec{q}_v + 2q_s\vec{q}_v^\intercal(\vec{x}\times\vec{y}) + q_s^2\vec{x}^\intercal\vec{y} \leqslant (\vec{q}_v^\intercal\vec{q}_v + q_s^2)\cos(\theta) \\
\cos(\theta) &\geqslant 2(\vec{q}_v^\intercal\vec{y})(\vec{q}_v^\intercal\vec{x}) - (\vec{x}^\intercal\vec{y})\vec{q}_v^\intercal\vec{q}_v + 2q_s\vec{q}_v^\intercal(\vec{x}\times\vec{y}) + q_s^2\vec{x}^\intercal\vec{y} \\
\cos(\theta) &\geqslant 2(\vec{q}_v^\intercal\vec{y})(\vec{q}_v^\intercal\vec{x}) + 2q_s\vec{q}_v^\intercal(\vec{x}\times\vec{y}) - (\vec{x}^\intercal\vec{q}_v)\vec{y}^\intercal\vec{q}_v + q_s^2\vec{x}^\intercal\vec{y} \\
\cos(\theta) &\geqslant 2(\vec{q}_v^\intercal\vec{y})(\vec{q}_v^\intercal\vec{x}) + 2q_s\vec{q}_v^\intercal(\vec{x}\times\vec{y}) - 2(\vec{x}^\intercal\vec{q}_v)\vec{y}^\intercal\vec{q}_v + (\vec{x}^\intercal\vec{q}_v)\vec{y}^\intercal\vec{q}_v + q_s^2\vec{x}^\intercal\vec{y} \\
\cos(\theta) &\geqslant 2(\vec{q}_v^\intercal\vec{y})(\vec{q}_v^\intercal\vec{x}) + 2q_s\vec{q}_v^\intercal(\vec{x}\times\vec{y}) - 2(\vec{x}^\intercal\vec{q}_v)\vec{y}^\intercal\vec{q}_v + \vec{x}^\intercal\vec{y} \\
\cos(\theta) &\geqslant \vec{x}^\intercal\vec{y} + 2(\vec{q}_v^\intercal\vec{y})(\vec{q}_v^\intercal\vec{x}) - 2(\vec{x}^\intercal\vec{y})\vec{q}_v^\intercal\vec{q}_v + 2q_s\vec{q}_v^\intercal(\vec{x}\times\vec{y}) \\
\cos(\theta) &\geqslant \vec{x}^\intercal\vec{y} + 2(\vec{q}_v^\intercal\vec{y})(\vec{q}_v^\intercal\vec{x}) - 2(\vec{x}^\intercal\vec{y})\vec{q}_v^\intercal\vec{q}_v + 2q_s\vec{x}^\intercal(\vec{y}\times\vec{q}_v)
\end{aligned}
$$

Appendix B

POSITIVE DEFINITENESS FOR HESSIAN OF CONTROL BARRIER FUNCTION

Then reiterating ∇T_1 and multiplying both sides by $\boldsymbol{q}^\intercal$ and $\boldsymbol{q}$ respectively:

$$\nabla T_1 = \frac{4k\boldsymbol{q}_r\boldsymbol{q}^\intercal M(\theta_C)}{\boldsymbol{q}^\intercal M(\theta_C)\boldsymbol{q}}$$
$$\boldsymbol{q}^\intercal\nabla T_1\boldsymbol{q} = \frac{4k}{\boldsymbol{q}^\intercal M(\theta_C)\boldsymbol{q}}\boldsymbol{q}^\intercal\left(\boldsymbol{q}_r\boldsymbol{q}^\intercal M(\theta_C)\right)\boldsymbol{q}$$

Repeating it for the individual terms of T_2 with some rearrangements:

$$\nabla T_2 = \frac{4k}{\boldsymbol{q}^\intercal M(\theta_C)\boldsymbol{q}}\boldsymbol{q}^\intercal\left(M(\theta_C)\boldsymbol{q}\boldsymbol{q}_r^\intercal\right)\boldsymbol{q} +$$
$$+ \left\|\boldsymbol{q}_r^* \otimes \boldsymbol{q} - \mathbf{1}\right\|^2\left(\frac{4k}{\left(\boldsymbol{q}^\intercal M(\theta_C)\boldsymbol{q}\right)^2}\boldsymbol{q}^\intercal\left(\left(\boldsymbol{q}^\intercal M(\theta_C)\right)^\intercal\boldsymbol{q}^\intercal M(\theta_C)\right)\boldsymbol{q} + \frac{-2k}{\boldsymbol{q}^\intercal M(\theta_C)\boldsymbol{q}}\boldsymbol{q}^\intercal M(\theta_C)\boldsymbol{q}\right)$$

Defining some new terms to make the system easier to simplify there are $X = \boldsymbol{q}_r^\intercal\boldsymbol{q}$ and

$Z = \boldsymbol{q}^\intercal M(\theta_C)\boldsymbol{q}$ and $\psi = \boldsymbol{q}^\intercal M(\theta_C)\boldsymbol{q} - \beta_1$. Then the above equations simplify to:

$$
\begin{aligned}
\boldsymbol{q}^\intercal \nabla^2 V_q(q) q &= \nabla T_1 + \nabla T_2 \\
&= \frac{4k}{\psi} \boldsymbol{q}^\intercal \left(\boldsymbol{q}_r \boldsymbol{q}^\intercal M(\theta_C)\right) q + \nabla T_2 \\
&= \frac{4k}{\psi} XZ + \nabla T_2 \\
&= \frac{4k}{\psi} XZ + \frac{4k}{\psi} \boldsymbol{q}^\intercal (\boldsymbol{q}_r \boldsymbol{q}^\intercal M(\theta_C)) q + (2 - 2\boldsymbol{q}_r^\intercal q) \frac{4k}{\psi^2} \boldsymbol{q}^\intercal (M(\theta_C) \boldsymbol{q}\boldsymbol{q}^\intercal M(\theta_C)) q \cdots \\
&- (2 - 2\boldsymbol{q}_r^\intercal) \frac{2k}{\psi} \boldsymbol{q}^\intercal M(\theta_C)\boldsymbol{q}) \\
&= \frac{4k}{\psi} XZ + \frac{4k}{\psi} XZ + (2 - 2X) \frac{4k}{\psi^2} Z^2 - (2 - 2X) \frac{2k}{\psi} Z) \\
&= \frac{4kZ}{\psi^2} \left(2XZ\psi + (1 - X)(2Z^2 - Z\psi)\right) \\
&= \frac{4kZ}{\psi^2} (2X\psi + (1 - X)(2Z - \psi)) \\
&= \gamma(2X\psi + (1 - X)(2Z - \psi)) \\
&= \gamma(2X(Z - \beta_1) + (1 - X)(2Z - (Z - \beta_1))) \\
&= \gamma(2XZ - 2X\beta_1 + (1 - X)(Z + \beta_1)) \\
&= \gamma(2XZ - 2X\beta_1 + Z + \beta_1 - XZ - X\beta_1) \\
&= \gamma(XZ - 2X\beta_1 + Z + \beta_1 - X\beta_1) \\
&= \gamma(X(Z - 3\beta_1) + Z + \beta_1)
\end{aligned}
$$

$$\boldsymbol{q}^\intercal \nabla^2 V_q \boldsymbol{q} = \gamma \left((\boldsymbol{q}_r^\intercal \boldsymbol{q})(\boldsymbol{q}^\intercal M(\theta_C)\boldsymbol{q} - 3\beta_1) + (\boldsymbol{q}^\intercal M(\theta_C)\boldsymbol{q} + \beta_1) \right)$$

$$\gamma = \frac{4k\boldsymbol{q}^\intercal M(\theta_C)\boldsymbol{q}}{(\boldsymbol{q}^\intercal M(\theta_C)\boldsymbol{q} - \beta_1)^2}$$

$$\gamma > 0$$

$$\boldsymbol{q}^\intercal M(\theta_C)\boldsymbol{q} + \beta_1 > 0$$

$$-1 \leqslant \boldsymbol{q}_r^\intercal \boldsymbol{q} \leqslant 1$$

$$\boldsymbol{q}^\intercal \nabla^2 V_q(\boldsymbol{q})\boldsymbol{q} > 0$$

Appendix C

ADDITIONAL GRAPHICAL RESULTS

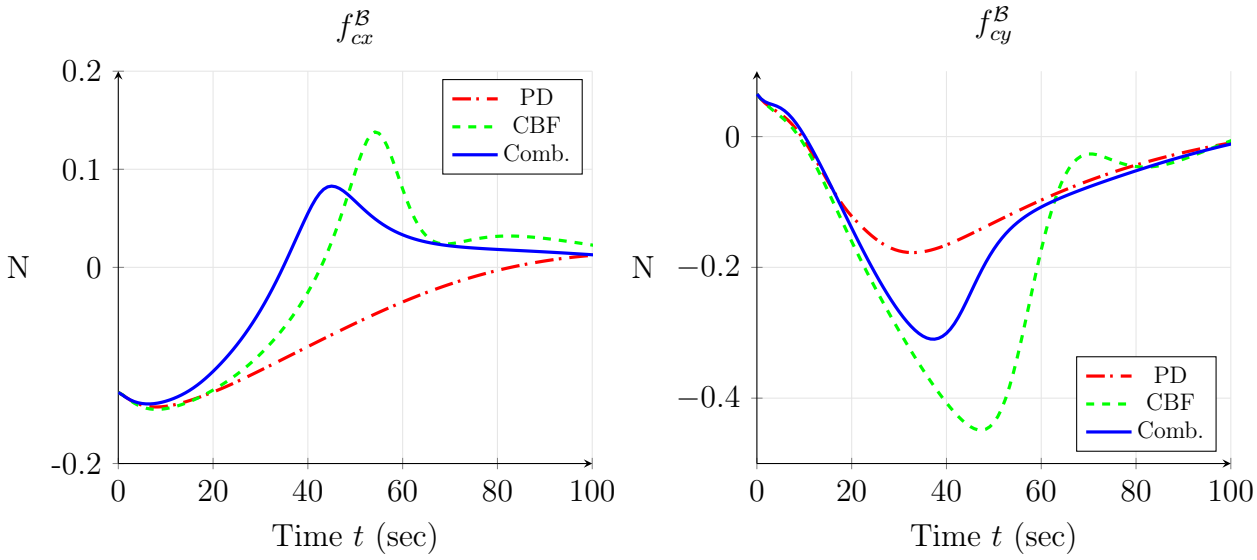

(a) Control in $\mathcal{B}_x$

(b) Control effort in $\mathcal{B}_y$

Figure C.1: Control comparison in $\mathcal{B}_x$ and $\mathcal{B}_y$: LEO

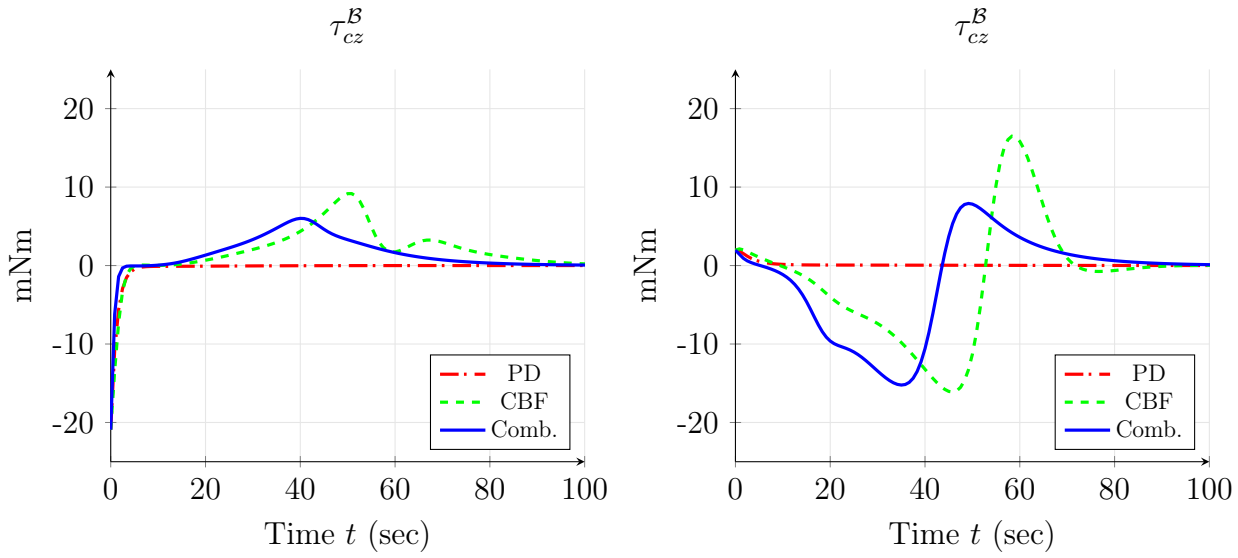

(a) Control torque in $\mathcal{B}_z$

(b) Control torque in $\mathcal{B}_y$

Figure C.2: Control torque comparison in $\mathcal{B}_z$ and $\mathcal{B}_y$: LEO

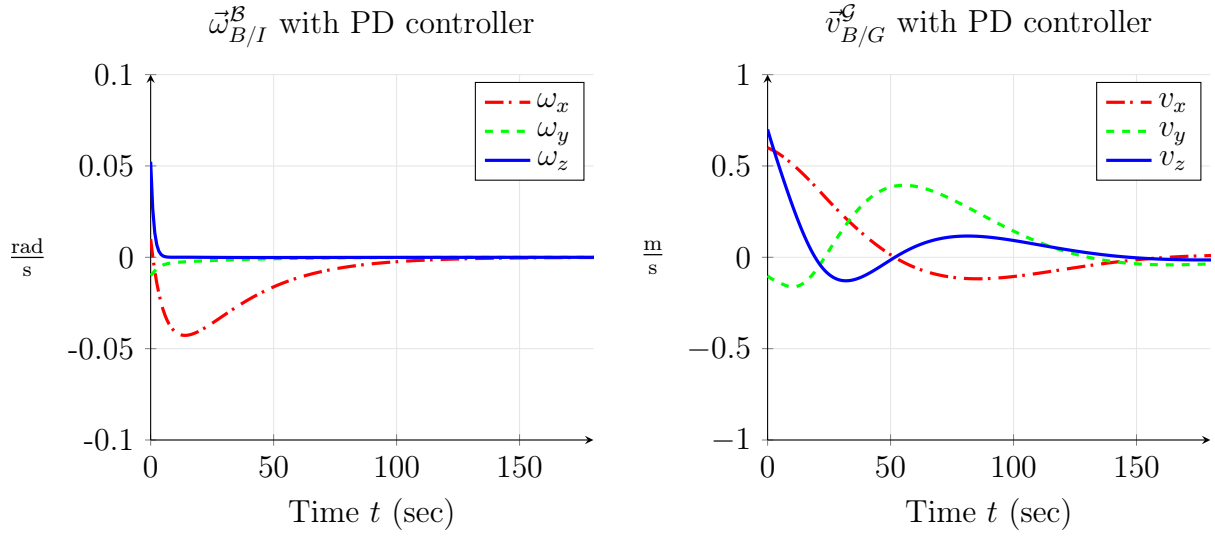

(a) Angular velocity in $\mathcal{B}$: PD

(b) Relative linear velocity in $\mathcal{B}$: PD

Figure C.3: Maratus Case with PD controller: Velocities over time

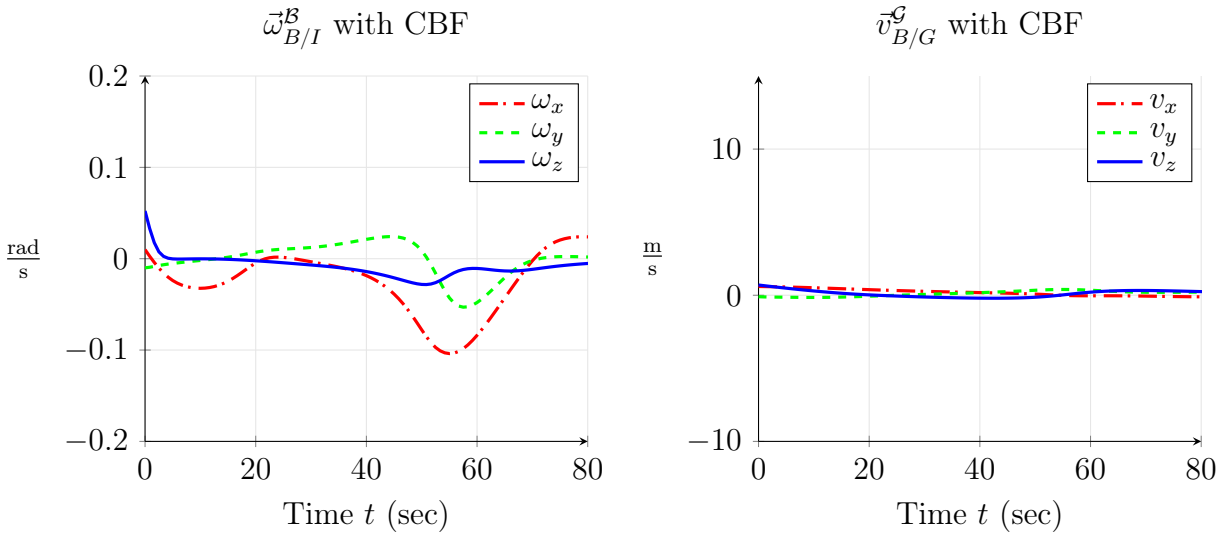

(a) Angular velocity in $\mathcal{B}$: CBF

(b) Relative linear velocity in $\mathcal{B}$: CBF

Figure C.4: Maratus Case with CBF: Velocities over time

VITA

Thomas is an aerospace engineer with a focus on Guidance, Navigation, and Control. Comments to tmkey@uw.edu or keythomasm@gmail.com.